Article

Multiple oestradiol functions inhibit ferroptosis and acute kidney injury

https://doi.org/10.1038/s41586-025-09389-x

Received: 12 November 2023

Accepted: 10 July 2025

Published online: 13 August 2025

Open access

Check for updates

Wulf Tonnus[1,29], Francesca Maremonti[2,29], Shubhangi Gavali[2,29], Marlena Nastassja Schlecht[1], Florian Gembardt[2], Alexia Belavgeni[3], Nadja Leinung[2], Karolin Flade[1], Natalie Bethe[1], Sofia Traikov[3,4], Anne Haag[5], Danny Schilling[6,7], Sider Penkov[8], Melodie Mallais[9], Christine Gaillet[10], Claudia Meyer[2], Melika Katebi[2], Anushka Ray[2], Louisa M. S. Gerhardt[2], Anne Brucker[1], Jorunn Naila Becker[1], Mirela Tmava[1], Lisa Schlicker[11], Almut Schulze[11], Nina Himmerkus[12], Andrej Shevchenko[4], Mirko Peitzsch[3], Uladzimir Barayeu[13], Sonia Nasi[14], Juliane Putz[15], Kenneth S. Korach[16], Joel Neugarten[17], Ladan Golestaneh[17], Christian Hugo[1], Jan Ulrich Becker[18], Joel M. Weinberg[19], Svenja Lorenz[20], Bettina Proneth[20], Marcus Conrad[20], Eckhard Wolf[21,22,23], Bernd Plietker[5], Raphaël Rodriguez[10], Derek A. Pratt[9], Tobias P. Dick[6,7], Maria Fedorova[8], Stefan R. Bornstein[24,25,26,27] & Andreas Linkermann[2,24,28] ✉

Acute tubular necrosis mediates acute kidney injury (AKI) and nephron loss[1], the hallmark of end-stage renal disease[2–4]. For decades, it has been known that female kidneys are less sensitive to AKI[5,6]. Acute tubular necrosis involves dynamic cell death propagation by ferroptosis along the tubular compartment[7,8]. Here we demonstrate abrogated ferroptotic cell death propagation in female kidney tubules. 17β-oestradiol establishes an anti-ferroptotic state through non-genomic and genomic mechanisms. These include the potent direct inhibition of ferroptosis by hydroxyoestradiol derivatives, which function as radical trapping antioxidants, are present at high concentrations in kidney tubules and, when exogenously applied, protect male mice from AKI. In cells, the oxidized hydroxyoestradiols are recycled by FSP1[9,10], but FSP1-deficient female mice were not sensitive to AKI. At the genomic level, female ESR1-deficient kidney tubules partially lose their anti-ferroptotic capacity, similar to ovariectomized mice. While ESR1 promotes the anti-ferroptotic hydropersulfide system, male tubules express pro-ferroptotic proteins of the ether lipid pathway which are suppressed by ESR1 in female tissues until menopause. In summary, we identified non-genomic and genomic mechanisms that collectively explain ferroptosis resistance in female tubules and may function as therapeutic targets for male and postmenopausal female individuals.

A broad review of 5.4 million Medicare recipients demonstrated a significantly lower AKI incidence in women[11]. Similarly, numerous clinical investigations have revealed a higher incidence of AKI and higher AKI-associated mortality for male individuals[12–15], especially in comparison to premenopausal women[16,17]. We hypothesized that such sex differences relate to sensitivity to acute tubular necrosis (ATN)[1], a hallmark of which is cell death by ferroptosis[18–20], a form of iron-catalysed necrosis and the predominant type of cell death in renal tubules in AKI[1,8,21]. In our hands, the sex differences after AKI induced by ischaemia–reperfusion injury (IRI) were even more pronounced than anticipated from the literature[16,22] (Fig. 1a,b). Importantly, the sex differences were phenocopied when we compared isolated renal tubules from male and female mice and assessed LDH release (Fig. 1c). We noted that the previously described cell death propagation in male tubules (Fig. 1d, Supplementary Fig. 1a,b and Supplementary Videos 1 and 2), which involves the loss of mitochondrial integrity (Supplementary Fig. 1c–e and Supplementary Video 3), was absent in female tubules (Fig. 1e,f, Supplementary Fig. 2a,b and Supplementary Video 4). Although the ferroptosis inhibitor ferrostatin-1 (Fer-1) prevented SYTOX positivity in male tubules, it had no significant effect on female tubules (Fig. 1g and Supplementary Video 5). Similarly, while Fer-1 reduced LDH release from male tubules, it did not protect female tubules (Fig. 1h). As a control, combined necroptosis- and pyroptosis-deficient kidney tubules isolated from *Mlkl* and *Gsdmd* double-knockout mice were assessed, and there was no significant difference compared with the wild-type littermates (Supplementary Fig. 2c). While male wild-type mice were previously demonstrated to be protected from IRI by Fer-1[8] or its more potent analogue UAMC-3203[23], these small molecules did not protect female mice from increases in serum urea and serum creatinine concentrations and from structural damage (Fig. 1i–l and Extended Data Fig. 1a–e). This result was consistent throughout various investigated doses of ischaemia before reperfusion (Extended Data Fig. 1f–i). *Gpx4*$^{fl/fl}$ *ROSA26-creER*^{T2} transgenic mice succumb within 14 days after activation of the Cre recombinase[20]. Compared with male littermates, less tubular necrosis (Extended Data Fig. 3a–c) was detected in such female mice alongside lower serum concentrations of creatinine and urea (Fig. 1m,n)

A list of affiliations appears at the end of the paper.

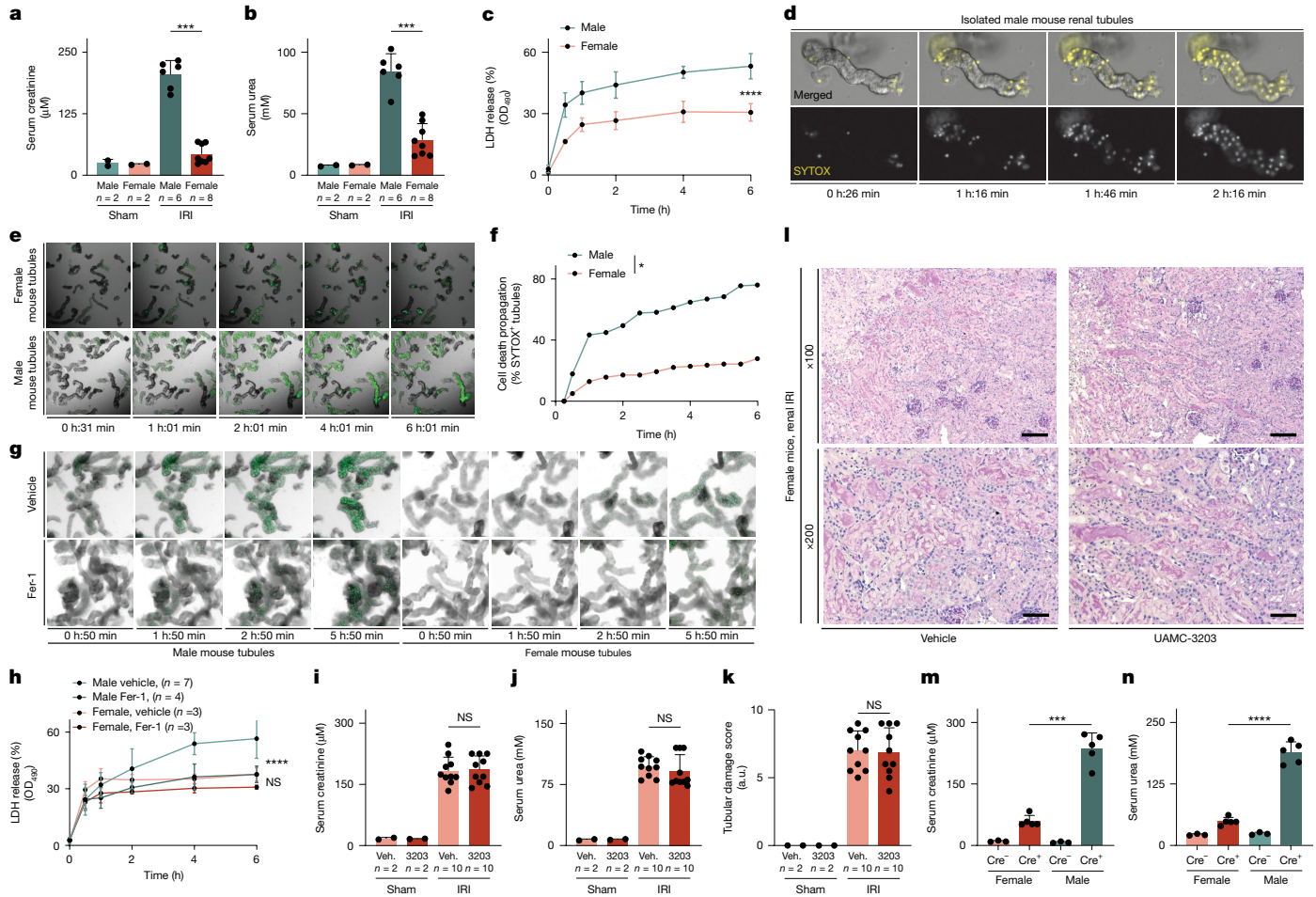

Fig. 1 | Female mice are resistant to AKI and renal tubular ferroptosis propagation. Male and female C57BL/6N mice underwent renal IRI (36 min). **a**,**b**, The serum levels of creatinine (**a**) and urea (**b**) after 48 h. **c**, Time-course analysis of LDH release from freshly isolated renal tubules of male and female mice. $n = 3$ mice per group. **d**, Still images of live imaging of cell death propagation using SYTOX Green (pseudocolour yellow). Single green channel images in greyscale were added to show the propagation of cell death. Representative of $n = 3$ individual experiments. **e**,**f**, Imaging (**e**) and quantification (**f**) of cell death propagation in male and female tubules. Representative of $n = 3$ individual experiments. **g**, Still images of delayed cell death propagation in male kidney tubules after addition of 5 μM Fer-1. Resistant female kidney tubules are depicted for control purposes. Representative of $n = 3$ biological replicates. **h**, The effect of Fer-1 on LDH release in male and female kidney tubules. **i**–**l**, Serum creatinine (**i**), serum urea (**j**) and tubular histology (quantification of tubular damage (**k**) and imaging (**l**)) of female wild-type (WT) mice pretreated with 10 mg per kg of the ferroptosis inhibitor UAMC-3203 (hard ischaemia). **m**,**n**, The serum levels of creatinine and urea 10 days after tamoxifen application obtained from *Gpx4*$^{fl/fl}$*ROSA26-creER*^{T2} transgenic mice. $n = 3$ (Cre$^-$) and 5 (Cre$^+$) mice per sex. $^*P < 0.05$, $^{**}P < 0.01$, $^{***}P < 0.001$, $^{****}P < 0.0001$. Scale bars, 50 μm (**l**, bottom) and 100 μm (**l**, top). Veh. vehicle.

10 days after tamoxifen application, but there was no significant difference in overall survival (Extended Data Fig. 3d). Concomitantly, no sex bias of tubular GPX4 expression was detected (Extended Data Fig. 3e). Collectively, these data indicate that ferroptotic cell death propagation is abrogated in female kidney tubules, and female kidney tubular tissue is endogenously resistant to ferroptosis.

Non-genomic anti-ferroptotic functions of oestradiol

We next investigated how sex hormones affect ferroptotic cell death. In ferroptosis-sensitive cell lines (HT1080 cells, NIH-3T3 cells and CD10 cells), testosterone treatment after cell death induction and testosterone pretreatment for 16 h had no significant effect on ferroptosis induction by all of the tested ferroptosis inducers (FINs; erastin, RSL3, FIN56 and FINO2) or ferroptocide (FTC) (Supplementary Figs. 3 and 4). By contrast, simultaneous treatment with either 17β-oestradiol or its hydroxylated derivative 2-hydroxyoestradiol (2OH-E2) protected from RSL3-induced ferroptosis (Fig. 2a,b). Consistent with previously published cell culture assays[24], 17β-oestradiol protected three ferroptosis-sensitive cell lines from ferroptosis induced by erastin, FIN56, FINO2 and FTC (Extended Data Fig. 4a–m). Comparable effects were detected after 16 h pretreatment (Extended Data Fig. 4a–g). We also investigated how persistent this effect was after RSL3-induced ferroptosis and detected no decrease in anti-ferroptotic potency until at least 6 h of treatment (Extended Data Fig. 5a,b). These data indicated that oestrogen rather than testosterone mediates ferroptosis resistance. Given that oestradiol and its hydroxylated derivative are phenols, we surmised that they inhibited lipid peroxidation as radical trapping antioxidants (RTAs), similarly to Fer-1 (and UAMC-3203)[25]. FENIX assays[26] demonstrated no RTA activity for cholesterol, testosterone and 17β-oestradiol, but showed potent activity of 2OH-E2 and 4OH-E2, comparable to the positive control PMC (2,2,5,7,8-pentamethyl-6-chromanol, a potent radical trap) (Fig. 2c–f and Extended Data Fig. 5c,d). We next established a liquid chromatography–mass spectrometry (LC–MS)-based strategy based on derivatization of the oestrogens (Extended Data Fig. 5e) to directly detect their levels in primary kidney tubular tissue (Methods). As expected, the content of E2 and OH-E2 (the peak encompassing both 2OH-E2 and 4OH-E2) was higher in the plasma of female mice compared with male mice, and the ratio of E2 to OH-E2 was 1:1 (Fig. 2g and Extended Data Fig. 5f). However, in renal

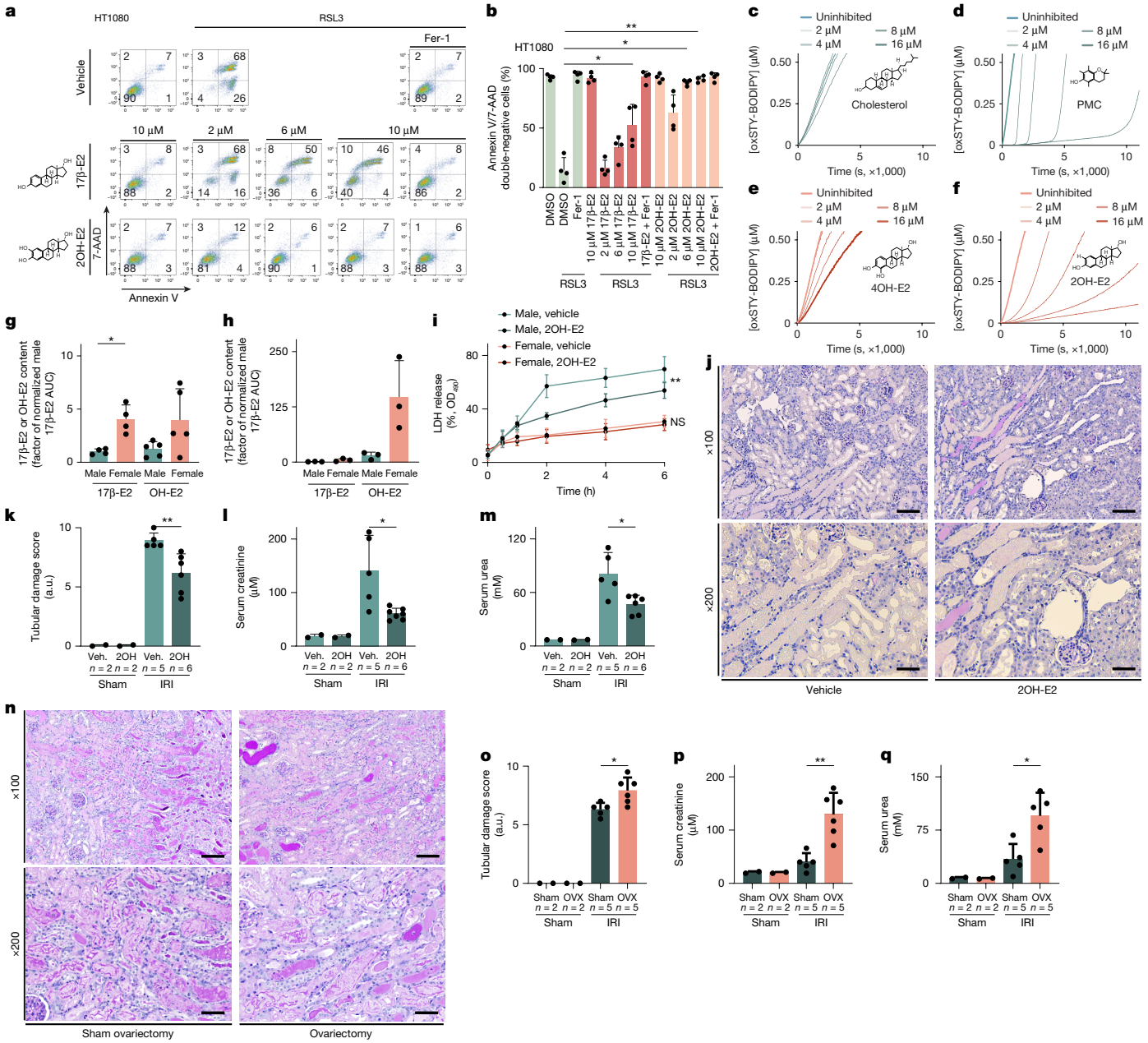

Fig. 2 | 2OH-E2 functions as a potent RTA to protect against ferroptosis propagation and accumulates in kidney tubules. a, HT1080 cells were simultaneously treated with the indicated doses of either 17β-oestradiol (17β-E2) or 2OH-E2 after ferroptosis induction by 1.13 μM RSL3. Representative flow cytometry analysis of annexin V/7-AAD was used as a cell death readout system. **b**, Quantification of cell death from **a**. $n = 4$ biological replicates per condition. **c**–**f**, FENIX assays for radical trapping activity including negative-control cholesterol (**c**) and positive-control PMC (a classical RTA) (**d**) as well as 17β-E2 (**e**) and 2OH-E2 (**f**). Representative of $n = 3$ biological replicates per condition. **g**,**h**, LC–MS detection of 17β-E2 or OH-E2 from mouse plasma ($n = 5$ mice per sex) (**g**) and freshly isolated mouse renal tubules ($n = 3$ samples per sex) (**h**) after derivatization with 3-pyridine sulfonyl (Methods). Data are normalized to the internal standard and 10^{-6} μg protein content. **i**, LDH release from male and female renal tubules after addition of 10 μM 2OH-E2. $n = 3$ mice per group. Male C57BL/6N mice underwent hard renal IRI after pretreatment with 10 mg per kg 2OH-E2. **j**–**m**, Tubular injury histology (imaging (**j**) and quantification (**k**)), and quantification of the serum levels of creatinine (**l**) and urea (**m**). **n**–**q**, Tubular injury histology (**n**) and quantification (**o**) and functional parameters (serum creatinine (**p**) and serum urea (**q**)) 48 h after medium IRI in female mice 7 days after sham surgery or ovariectomy (OVX). Scale bars, 50 μm (**j** and **n**, bottom) and 100 μm (**j** and **n**, top).

tubules, the levels of E2 and OH-E2 were higher in female mice compared with in male mice and, unexpectedly, the ratio of E2 to OH-E2 was substantially offset to OH-E2, demonstrating OH-E2 accumulation in this compartment (Fig. 2h and Extended Data Fig. 5f). We hypothesized that, with such content, 2OH-E2 may protect kidney tubular tissue from ferroptosis in a non-genomic manner. To test this, we treated male and female kidney tubules with exogenous 2OH-E2. Whereas male tubules exhibited significantly less LDH-release and cell death propagation, 2OH-E2 did not further protect female tubules (Fig. 2i). The potency was comparable to Fer-1 (Fig. 1h), which can be rationalized based on the similar potency kinetics with which 2OH-E2 ($k_{inh} = 1.0 \times 10^4 \pm 0.1 \times 10^4\ M^{-1}\ s^{-1}$) and Fer-1 ($k_{inh} = 8.2 \times 10^4 \pm 0.3 \times 10^4\ M^{-1}\ s^{-1}$) react with propagating lipid peroxyl radicals in phospholipid bilayers as demonstrated by a FENIX assay[27]. The RTA basis of the anti-ferroptotic activity of 2OH-E2 was corroborated by findings with a newly generated simplified dihydrobenzene structure (5,6,7,8-tetrahydronaphthalene-2,3-diol),

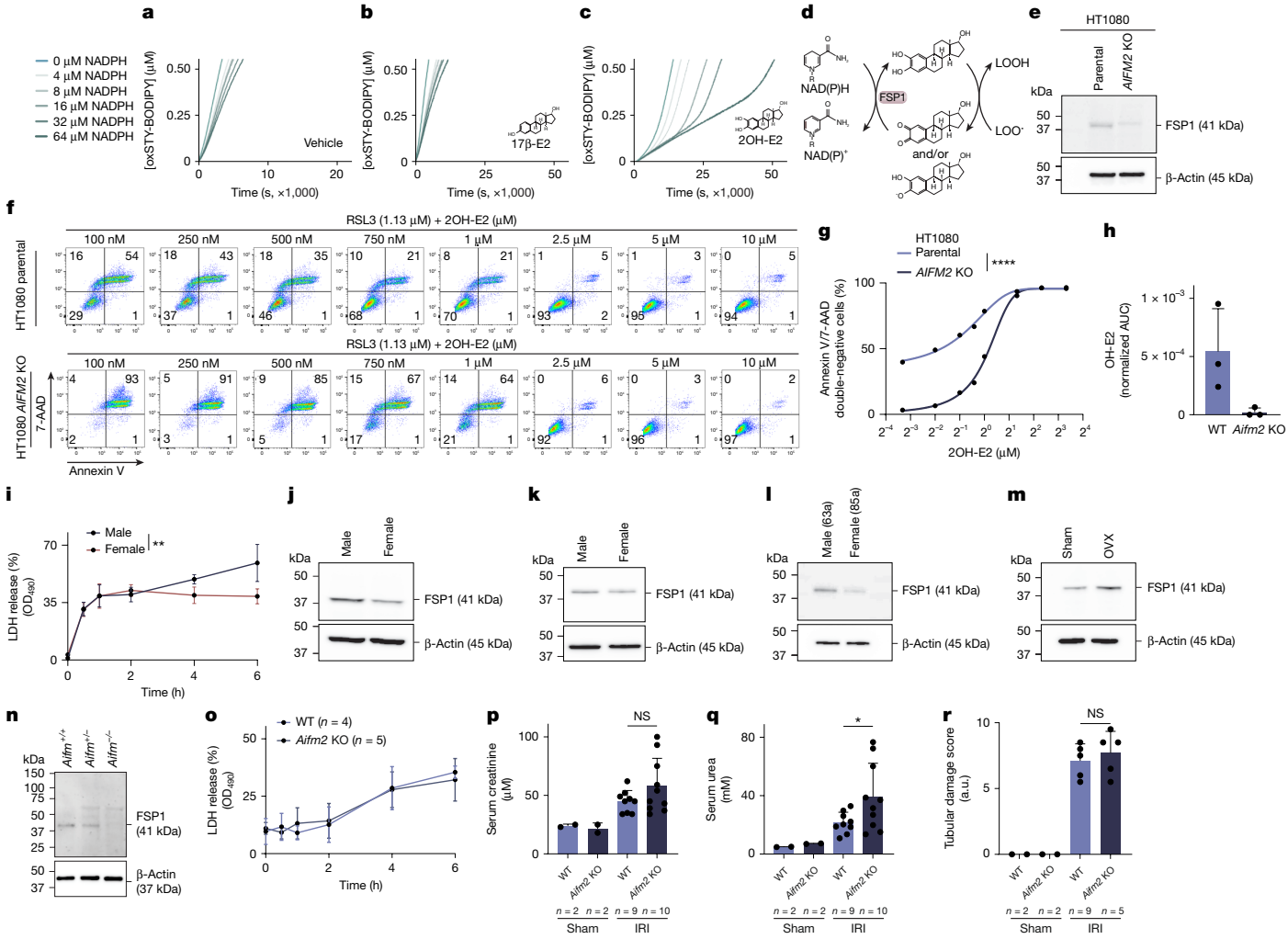

Fig. 3 | FSP1 regenerates oxidized oestradiol derivatives to enhance anti-ferroptotic activity in cells. a–**c**, FENIX assays were performed after addition of 16 μM mFSP1, 320 nM FAD and the indicated doses of NADPH to assess inhibition of radical trapping activity for vehicle solution (**a**), 17β-E2 (**b**) or 2OH-E2 (**c**). Representative of $n = 3$ biological eplicates. **d**, FSP1 recycles oestradiol derivates. **e**, Western blot analysis of CRISPR-mediated knockout (KO) of *AIFM2* in HT1080 cells. **f**,**g**, Imaging (**f**) and quantification (**g**) of dose–response experiments of 2OH-E2 after incubation with RSL3 in parental and *AIFM2*-knockout HT1080 cells. $n = 4$ biological replicates. **h**, Analysis of OH-E2 content from freshly isolated wild-type and FSP1-deficient (*Aifm2*-KO) female mouse tubules. $n = 3$ biological replicates per group. **i**, LDH release of *Aifm2*-knockout tubules isolated from male or female mice. $n = 3$ mice per group. **j**, Western blot analysis of FSP1 in freshly isolated male and female tubules from mice (**j**), pigs (**k**) and humans (**l**) (individual 85a is considered postmenopausal). **m**, Western blot analysis of FSP1 in mouse tubules 7 days after sham surgery or ovariectomy. **n**, Western blot analysis of loss of FSP1 protein expression in *Aifm2*-knockout female mouse tubules. **o**, LDH release from female FSP1-deficient (*Aifm2*KO) or wild-type littermate tubules. **p**–**r**, The levels of serum creatinine (**p**) and serum urea (**q**) and tubular injury scoring (**r**) 48 h after medium IRI in wild-type or FSP1-deficient (*Aifm2*KO) female mice.

which was similarly potent to 2OH-E2 in cell culture (Extended Data Fig. 6a–c). To test the potency of exogenous 2OH-E2 in an in vivo setting, we applied 2OH-E2 to our standard assay of kidney IRI. As demonstrated in Fig. 2k–n and Extended Data Fig. 5g,h, 2OH-E2 indeed protected male mice in all readout systems tested in this model. Consistent with this finding, ovariectomized mice became sensitive to IRI (Fig. 2o–r and Extended Data Fig. 5i). Catechols can form complexes with iron potentially affecting its reactivity[28]. We therefore investigated the iron-binding potential of the hydroxyoestrogen derivatives and found that 4OH-E2 can function as a weak iron chelator while 2OH-E2 does not (Supplementary Fig. 5). These data suggest that the non-genomic anti-ferroptotic effects of oestrogens result from RTA activity rather than iron-chelating properties.

FSP1 recycles hydroxyoestradiols

We wondered whether hydroxyoestradiol derivatives, after undergoing oxidation to the corresponding quinones, can be regenerated by FSP1 (encoded by *AIFM2*), as demonstrated for coenzyme Q10 and vitamin K[10,29]. The addition of recombinant FSP1 to the FENIX assays resulted in a potentiation of RTA activity among all oestradiol derivatives tested (Fig. 3a–c and Extended Data Fig. 6d–i). We therefore propose an NADPH-dependent regenerative mechanism of oestradiol regeneration (Fig. 3d). Similar effects were obtained in cell-free systems in which ascorbate or superoxide thermal source-1 (SOTS-1) were tested for their ability to regenerate oestradiol derivatives (Extended Data Fig. 6j–q). We generated a CRISPR–Cas9-mediated knockout of *AIFM2* (encoding FSP1) in HT1080 cells (Fig. 3e) and tested the required anti-ferroptotic dose of 2OH-E2 in parental and knockout cells (Fig. 3f,g and Extended Data Fig. 7a). To obtain 50% annexin-V/7-AAD double negativity, the required dose in parental cells was 750 nM 2OH-E2, whereas the knockout cells required at least 2.5 μM, and the content of reduced OH-E2, but not E2, was about 100 times lower in FSP1-deficient mice (Fig. 3h and Extended Data Fig. 8a). In endogenously ferroptosis-resistant HT29 cells, the knockout of *AIFM2* sensitized the cells to RSL3-induced ferroptosis (Extended Data Fig. 7b–e). We also investigated a specific

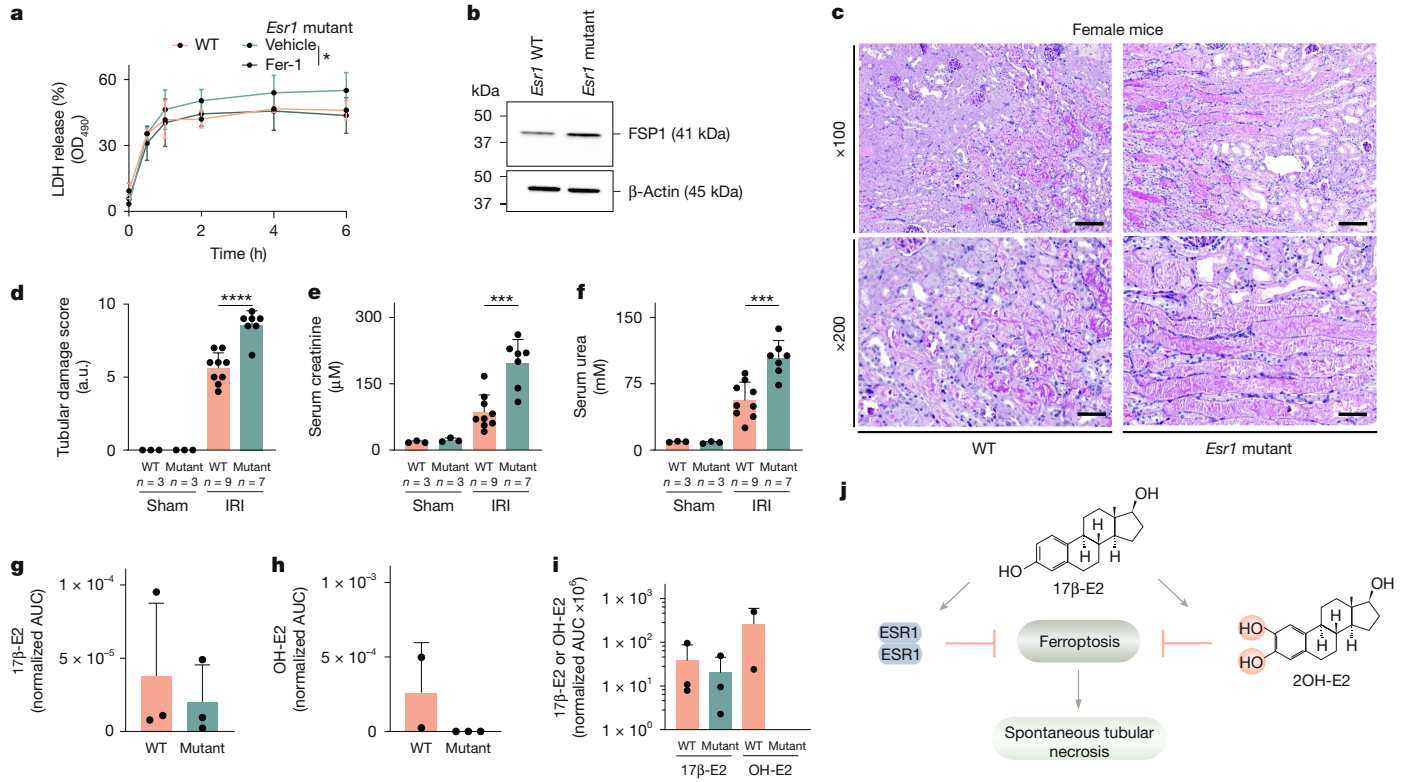

Fig. 4 | *Esr1* deficiency sensitizes to tubular ferroptosis and AKI. Renal tubules were freshly isolated from both wild-type and mutant *Esr1* littermate female mice. **a**, LDH release from mouse tubules. $n = 3$ mice per group. **b**, Western blot analysis of FSP1 from either wild-type or ESR1-deficient (*Esr1* mutant) female mouse tubules. **c**,**d**, Imaging (**c**) and quantification (**d**) of tubular injury 48 h after hard IRI in ESR1-deficient (mutant) female mice or wild-type littermates. **e**,**f**, Corresponding serum levels of creatinine (**e**) and urea (**f**). **g**,**h**, Renal tubular levels of 17β-E2 (**g**) and OH-E2 (**h**). $n = 3$ mice per group. **i**, Logarithmic transformation of the data presented in **g** and **h**, normalized per 10^{-6} μg protein content. **j**, The working model, demonstrating that oestrogens suppress ferroptosis both through genomic and non-genomic functions.

FSP1 inhibitor (viFSP1) in HT1080 cells and HT29 cells with similar results (Extended Data Fig. 7f,g). Likewise, other FSP1 inhibitors sensitized otherwise resistant female cell lines (HT29 and HeLa cells) to ferroptosis (Extended Data Fig. 7h,i). Consistent with these results, the aromatase inhibitor anastrozole sensitized HeLa cells to ferroptosis, and additional treatment with viFSP1 did not further sensitize those cells (Extended Data Fig. 7j). However, the sex differences described above for kidney tubules were not fully reversed by FSP1 deficiency (Fig. 3i), which prompted us to investigate the overall expression of FSP1 in male and female renal tubules. In tubular lysates obtained from mice, pigs and humans, FSP1 expression was higher in male animals (Fig. 3j–l). Consistent with these data, FSP1 expression in female tubules increased after ovariectomies (Fig. 3m). We confirmed the antibody specificity in wild-type, heterozygous and *Aifm2*-knockout mice (Fig. 3n). In the kidney tubular LDH-release assay, neither *Aifm2* knockout nor three different viFSP1 doses tested exhibited significant differences (Fig. 3o and Extended Data Fig. 8b), suggesting the presence of additional anti-ferroptotic systems in the tubular compartment. Consistent with this hypothesis, we observed a non-significant trend toward sensitization in female FSP1-deficient (*Aifm2*-knockout) mice in the kidney IRI model (Fig. 3p–r and Extended Data Fig. 8c). We therefore investigated potential compensatory mechanisms in the FSP1-deficient mouse tubules. While GPX4 and ACSL4 were unaffected by the *Aifm2* knockout, we found increased levels of the thioredoxin system (thioredoxin (TRX) and peroxiredoxin 1 (PRX1)) in male and female mice (Extended Data Fig. 8d,e). After inhibition of the PRX1 pathway (which also involves thioredoxin reductase 1) with FTC[30], we unleashed hypersensitivity, detecting unusually high levels of LDH release from isolated tubules that was entirely reversed by the addition of Fer-1 in female *Aifm2*-knockout mice (Extended Data Fig. 8f). However, FTC also sensitized wild-type female tubules (Extended Data Fig. 8g). These data demonstrate how the anti-ferroptotic activity of individual systems in cultured cells, such as FSP1, cannot be easily extrapolated to the complex in vivo environment in which several ferroptosis surveillance systems co-exist to collectively inhibit ferroptosis in female kidney tubules. Thus, to better understand ferroptosis regulation in vivo beyond the potent non-genomic functions of hydroxyoestradiol derivatives, we extended our investigation on genomic functions of oestradiol mediated through ESR1.

Genomic anti-ferroptotic functions of oestradiol

We bred ESR1-deficient heterozygous mice to obtain parental littermates (both wild-type and heterozygous) and ESR1-deficient mice. Isolated kidney tubules of female ESR1-deficient mice demonstrated higher LDH release compared with co-housed wild-type littermates (Fig. 4a) and treatment with Fer-1 reversed this increase to the level of untreated wild-type mice (Fig. 4a). Consistent with Fig. 3j–m, FSP1 protein expression in tubular lysates of ESR1-mutant mice was increased (Fig. 4b). As expected from the tubule experiment, ESR1-deficient female mice were significantly more sensitive to kidney IRI (Fig. 4c–f). Notably, while these mice phenocopied the 17β-oestradiol levels of wild-type mice, hydroxyoestradiols were undetectable in the tubules of ESR1-deficient mice (Fig. 4g–i). As ESR1 dysfunction correlates with the absence of 2OH-E2 and hypersensitivity to ferroptosis, regardless of the upregulation of FSP1, this approach enabled us to differentiate genomic from non-genomic functions of oestradiols (Fig. 4j). As expected, a potent ferrostatin exhibited protective effects after IRI in ESR1-deficient female

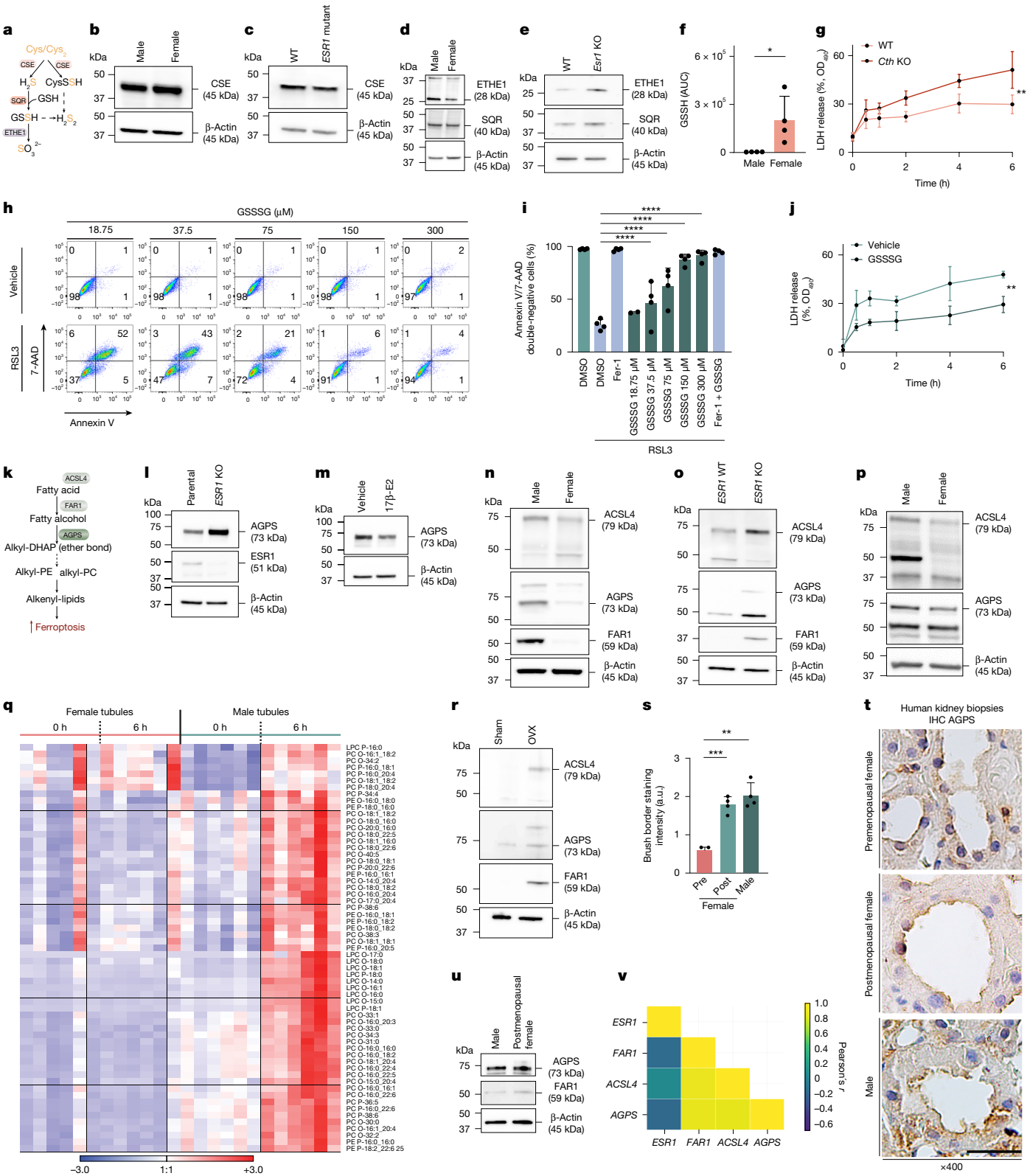

Fig. 5 | See next page for caption.

mice (Extended Data Fig. 9a–d). Collectively, these data demonstrate that ESR1 contributes at the genomic level to the anti-ferroptotic state of female kidney tubules. However, the regulation of FSP1 did not fully explain the sex differences in AKI sensitivity, which led us to investigate other genomically regulated, ESR1-dependent ferroptosis regulating systems.

As genes involved in generation of anti-ferroptotic hydropersulfides/polysulfides[31,32] are predicted to be strongly influenced by ESR1 expression[33], we hypothesised that these might contribute to the protection of female kidney tubules, potentially in an ESR1-dependent manner (Fig. 5a). After assessment of the protein expression levels of CSE, a major regulator of hydropersulfide generation, no difference was

Fig. 5 | ESR1 limits hydropersulfide degradation and ether lipid plasticity. **a**, Hydropersulfide metabolism is controlled by CSE, SQR and ETHE1. **b**,**c**, Western blot analysis of CSE protein levels from ESR1-deficient (mutant) and wild-type female isolated tubules (**b**) and in male and female tubules (**c**). **d**,**e**, ETHE1 and SQR expression in male and female (**d**) and wild-type and *Esr1*-knockout (**e**) mouse tubules. **f**, Quantification of GSSH in male and female mouse tubules. $n = 4$ biological replicates per group. **g**, LDH release over time from wild-type and *Cth*-knockout female mouse tubules. **h**,**i**, GSSSG dose-dependently prevents ferroptosis in HT1080 cells. $n = 3$ individual experiments. **j**, LDH release over time from male mouse tubules after addition of either vehicle solution or 50 µM GSSSG. $n = 3$ mice per group. **k**, Investigated proteins involved in the ether lipid production pathway. **l**, Protein expression of AGPS in ESR1-deficient (*ESR1* KO) HT29 cells compared with in parental cells. **m**, Protein expression of AGPS after treatment with 17β-E2 for 16 h in HT29 cells. **n**,**o**, Protein expression of ACSL4, AGPS and FAR1 in mouse male and female tubular lysates (**n**) and in mouse female wild-type and ESR1-deficient tubular lysates (**o**). **p**, Protein expression of ACSL4 and AGPS in porcine male and female renal tubular lysates. **q**, Untargeted lipidomics in mouse kidney tubules during spontaneous tubular ferroptosis. Colour scale is semi-quantitative, as described in Methods. $n = 6$ individual experiments per sex. **r**, Protein expression of ACSL4, AGPS and FAR1 in freshly isolated kidney tubules obtained from sham and ovariectomized mice (artificial induction of a postmenopausal state). **s**,**t**, Quantification of AGPS immunohistochemistry staining intensity in renal biopsies of premenopausal (pre) and postmenopausal (post) female as well as male patients ($n = 4$ individuals per group) (**s**) exemplified by representative specimens (**t**). **u**, AGPS and FAR1 protein levels in tubules from male and postmenopausal female individuals. **v**, Correlation heat map of *ESR1* as well as *FAR1*, *ACSL4* and *AGPS* from $ESR1^+$ breast cancer cell lines. PC, phosphatidylcholine; PE, phosphatidylethanolamine. Scale bars, 25 µm (**t**).

observed between the sexes (Fig. 5b,c). However, hydropersulfides are degraded through ETHE1 downstream of SQR. The protein expression in kidney tubules was found to be upregulated in male mice (Fig. 5d) and ESR1-deficient female mice (Fig. 5e), suggesting a more efficient turnover of the hydropersulfides in male mice. Indeed, higher levels of the glutathione hydropersulfide GSSH, a known suppressor of ferroptosis[31,32], were present in female tubules (Fig. 5f) while GSH levels and other hydropersulfides were not significantly different (Extended Data Fig. 9e–h). Likewise, the addition of oestrogens to HT29 cells resulted in higher levels of GSSH while GSH again remained unchanged (Extended Data Fig. 9i). Indeed, tubules isolated from CSE-deficient female mice (*Cth*-knockout mice) exhibited higher levels of LDH release compared with the wild-type littermates (Fig. 5g), whereas *Cth*-knockout male mice were unaffected (Extended Data Fig. 9j). In cell culture, the incubation of HT1080 cells with glutathione trisulfide (GSSSG; a precursor of hydropersulfides) protected these cells from both erastin-induced (Extended Data Fig. 9k,l) and RSL3-induced (Fig. 5h,i) ferroptosis. Similarly, male tubules were protected from LDH-release after GSSSG treatment (Fig. 5j and Extended Data Fig. 9m). These data indicate that ESR1-dependent downregulation of hydropersulfide degeneration represents one mechanism of a genomic oestrogen-mediated anti-ferroptotic outcome in female kidney tubules. Moreover, these data introduce the importance of the anti-ferroptotic capacity of the hydropersulfide system in an in vivo setting.

In contrast to hydropersulfides, the plasticity of ether lipids has recently been demonstrated to sensitize mouse tumours to ferroptosis[34], but a potential role in acute tissue injury was not assessed. We therefore investigated the key enzymes in the ether-lipid-production pathway (Fig. 5k). Knockout of *ESR1* in HT29 cells, which are known to be insensitive to classical FINs, led to a prominent upregulation of AGPS, the only known protein to generate the ether bond, compared with parental cells (Fig. 5l). Vice versa, we observed AGPS downregulation after incubation with E2 (Fig. 5m). Consistent with a previous report[35], CRISPR–Cas9-mediated knockout of *FAR1* in CD10 cells and HT1080 cells did not desensitize cells to ferroptosis induced by any of the FINs tested (Extended Data Fig. 10a–f). However, the tubular protein expression of ACSL4, FAR1 and AGPS was all upregulated in male and ESR1-deficient female tubules (Fig. 5n,o). Although we failed to establish an anti-porcine FAR1 antibody, similar effects for ACSL4 and AGPS were documented from freshly isolated pig tubules (Fig. 5p), suggesting that this effect was conserved during mammalian evolution. This encouraged us to directly compare the lipidomes of freshly isolated male and female tubules over time. First, we found higher levels of ether lipids in tubules of male mice under basal conditions (Extended Data Fig. 10g). Importantly, ether phospholipids were markedly increased during the process of tubular injury only in male kidney tubules (Fig. 5q), while corresponding ester phospholipids, used as controls, did not exhibit a comparable pattern (Extended Data Fig. 10h). These data indicated that the pro-ferroptotic plasticity of ether lipids is a specific feature of male but not female tubules, and that the ether-lipid-production pathway is suppressed in an ESR1-dependent manner. We therefore speculated that this inhibition would be lost after the menopause. Indeed, when we investigated the artificial postmenopausal system of ovariectomy in mice to test AGPS and FAR1 expression, higher levels of AGPS and FAR1 were detected at the protein level compared with in sham-operated female mice (Fig. 5r). Consistent with this observation, immunohistochemistry analysis of AGPS in a set of human kidney biopsies demonstrated AGPS protein expression in the brush borders of proximal renal tubules of male and postmenopausal female specimens and, to a much lesser extent, in samples obtained from premenopausal women (Fig. 5s,t). Likewise, in lysates of freshly isolated human kidney tubules obtained from postmenopausal female or male patients, expression of AGPS and FAR1 were comparable (Fig. 5u). More generally, our data are consistent with a publicly available human kidney single-cell transcriptome database in which the expression of *ACSL4*, *FAR1* and *AGPS* in proximal tubules was higher in AKI samples compared with in healthy control samples[36] (Extended Data Fig. 10i). Finally, the effects of ESR1 are best studied in the context of breast cancer. We compared expression of *ACLS4*, *FAR1* and *AGPS*, respectively, in $ESR1^+$ and $ESR1^-$ breast cancer cell lines and detected a strong inverse correlation of all three genes with *ESR1* expression[37] (Fig. 5v and Extended Data Fig. 10j). We conclude that ether lipids and their plasticity are indeed involved in hypersensitive male individuals and contribute to kidney tubular damage, while this pro-ferroptotic signal is suppressed in female individuals before menopause in an ESR1-dependent manner. The robustness of this correlation is reflected in a study on premenopausal female patients undergoing hormone deprivation, which lead to marked increases in circulating ether lipid species[38]. In summary, male and postmenopausal female kidney tubules are sensitized to ferroptosis and ATN by plasticity of ether lipids while the production of hydropersulfides functions as an anti-ferroptotic system in female individuals.

Discussion

In 1988, it was first observed that daily intraperitoneal injections of ferric nitrilotriacetate resulted in the death of all male mice within 6 days, whereas all female and castrated male mice survived 3 months of treatment[39]. Moreover, ferroptosis-mediated effects after iron application recently indicated a role of iron in the damaging process of solid organs including the kidneys[23]. Here we identified genomic and non-genomic mechanisms that explain decreased ferroptosis sensitivity in female individuals. We highlight a predominant role in ferroptosis propagation during ATN in male mice (Supplementary Fig. 1). While oestradiols and hydropersulfides protect female tubules, male individuals are hypersensitive due to increased plasticity of ether lipids. These delicate intertwined anti-ferroptotic systems suggest ferroptosis targeting to be of particular benefit for the prevention

of AKI in male and postmenopausal female individuals. In conclusion, ferroptosis sensitivity explains the higher susceptibility of male individuals to AKI.

It is notable that the FSP1 protein expression positively correlates with ferroptosis sensitivity, and that female tissues appear to express less of it. We previously demonstrated similar counterintuitive effects for the GPX4 system in highly ferroptosis-sensitive tissues, such as the adrenals[40]. This indicates plasticity of anti-ferroptotic systems and is consistent with our findings of increased production of hydropersulfides that may provide ferroptosis resistance in response to lower FSP1 expression. Along similar lines, ESR1-dependent suppression of ether lipid plasticity may compensate for lower FSP1 expression.

A limitation of our study relates to our tubule-isolation protocol, which is performed using an ex vivo model. However, cell death propagation was recently detected directly by longitudinal intravital imaging after IRI[41], confirming that the cell death propagation pattern investigated here occurs in male mice in situ in a similar manner. Finally, our experiments indicate a role of ferroptosis in kidney and potentially other solid organ transplantation, including the possibility to target ferroptosis for the purpose of prevention of cell death and necroinflammation[42], predominantly in male and postmenopausal female organs.

Online content

Any methods, additional references, Nature Portfolio reporting summaries, source data, extended data, supplementary information, acknowledgements, peer review information; details of author contributions and competing interests; and statements of data and code availability are available at https://doi.org/10.1038/s41586-025-09389-x.

1. Maremonti, F., Meyer, C. & Linkermann, A. Mechanisms and models of kidney tubular necrosis and nephron loss. *J. Am. Soc. Nephrol.* **33**, 472–486 (2022).
2. Kellum, J. A. et al. Acute kidney injury. *Nat. Rev. Dis. Primers* **7**, 52 (2021).
3. Sharfuddin, A. A. & Molitoris, B. A. Pathophysiology of ischemic acute kidney injury. *Nat. Rev. Nephrol.* **7**, 189–200 (2011).
4. Venkatachalam, M. A., Weinberg, J. M., Kriz, W. & Bidani, A. K. Failed tubule recovery, AKI-CKD Transition, and kidney disease progression. *J. Am. Soc. Nephrol.* **26**, 1765–1776 (2015).
5. Park, K. M., Kim, J. I., Ahn, Y., Bonventre, A. J. & Bonventre, J. V. Testosterone is responsible for enhanced susceptibility of males to ischemic renal injury. *J. Biol. Chem.* **279**, 52282–52292 (2004).
6. Silbiger, S. R. & Neugarten, J. The impact of gender on the progression of chronic renal disease. *Am. J. Kidney Dis.* **25**, 515–533 (1995).
7. Belavgeni, A., Meyer, C., Stumpf, J., Hugo, C. & Linkermann, A. Ferroptosis and necroptosis in the kidney. *Cell Chem. Biol.* **27**, 448–462 (2020).
8. Linkermann, A. et al. Synchronized renal tubular cell death involves ferroptosis. *Proc. Natl Acad. Sci. USA* **111**, 16836–16841 (2014).
9. Bersuker, K. et al. The CoQ oxidoreductase FSP1 acts parallel to GPX4 to inhibit ferroptosis. *Nature* **575**, 688–692 (2019).
10. Doll, S. et al. FSP1 is a glutathione-independent ferroptosis suppressor. *Nature* **575**, 693–698 (2019).
11. Xue, J. L. et al. Incidence and mortality of acute renal failure in Medicare beneficiaries, 1992 to 2001. *J. Am. Soc. Nephrol.* **17**, 1135–1142 (2006).
12. Bagshaw, S. M. et al. Prognosis for long-term survival and renal recovery in critically ill patients with severe acute renal failure: a population-based study. *Crit. Care* **9**, R700–R709 (2005).
13. Chertow, G. M. et al. Predictors of mortality and the provision of dialysis in patients with acute tubular necrosis. The Auriculin Anaritide Acute Renal Failure Study Group. *J. Am. Soc. Nephrol.* **9**, 692–698 (1998).
14. Cosentino, F., Chaff, C. & Piedmonte, M. Risk factors influencing survival in ICU acute renal failure. *Nephrol. Dial. Transpl.* **9**, 179–182 (1994).
15. Mehta, R. L., Pascual, M. T., Gruta, C. G., Zhuang, S. & Chertow, G. M. Refining predictive models in critically ill patients with acute renal failure. *J. Am. Soc. Nephrol.* **13**, 1350–1357 (2002).
16. Chesnaye, N. C., Carrero, J. J., Hecking, M. & Jager, K. J. Differences in the epidemiology, management and outcomes of kidney disease in men and women. *Nat. Rev. Nephrol.* **20**, 7–20 (2024).
17. Dines, V. A. & Garovic, V. D. Menopause and chronic kidney disease. *Nat. Rev. Nephrol.* **20**, 4–5 (2024).
18. Dixon, S. J. et al. Ferroptosis: an iron-dependent form of nonapoptotic cell death. *Cell* **149**, 1060–1072 (2012).
19. Dixon, S. J. & Olzmann, J. A. The cell biology of ferroptosis. *Nat. Rev. Mol. Cell Biol.* **25**, 424–442 (2024).
20. Friedmann Angeli, J. P. et al. Inactivation of the ferroptosis regulator Gpx4 triggers acute renal failure in mice. *Nat. Cell Biol.* **16**, 1180–1191 (2014).
21. Tonnus, W. et al. Dysfunction of the key ferroptosis-surveilling systems hypersensitizes mice to tubular necrosis during acute kidney injury. *Nat. Commun.* **12**, 4402 (2021).
22. Ide, S. et al. Sex differences in resilience to ferroptosis underlie sexual dimorphism in kidney injury and repair. *Cell Rep.* **41**, 111610 (2022).
23. Van Coillie, S. et al. Targeting ferroptosis protects against experimental (multi)organ dysfunction and death. *Nat. Commun.* **13**, 1046 (2022).
24. Mishima, E. et al. Drugs repurposed as antiferroptosis agents suppress organ damage, including AKI, by functioning as lipid peroxyl radical scavengers. *J. Am. Soc. Nephrol.* https://doi.org/10.1681/asn.2019060570 (2019).
25. Zilka, O. et al. On the mechanism of cytoprotection by ferrostatin-1 and liproxstatin-1 and the role of lipid peroxidation in ferroptotic cell death. *ACS Cent. Sci.* **3**, 232–243 (2017).
26. Shah, R., Farmer, L. A., Zilka, O., Van Kessel, A. T. M. & Pratt, D. A. Beyond DPPH: use of fluorescence-enabled inhibited autoxidation to predict oxidative cell death rescue. *Cell Chem. Biol.* **26**, 1594–1607 (2019).
27. Poon, J. F., Zilka, O. & Pratt, D. A. Potent ferroptosis inhibitors can catalyze the cross-dismutation of phospholipid-derived peroxyl radicals and hydroperoxyl radicals. *JACS* **142**, 14331–14342 (2020).
28. Bijlsma, J. et al. Revealing the main factors and two-way interactions contributing to food discolouration caused by iron-catechol complexation. *Sci. Rep.* **10**, 8288 (2020).
29. Mishima, E. et al. A non-canonical vitamin K cycle is a potent ferroptosis suppressor. *Nature* **608**, 778–783 (2022).
30. Llabani, E. et al. Diverse compounds from pleuromutilin lead to a thioredoxin inhibitor and inducer of ferroptosis. *Nat. Chem.* **11**, 521–532 (2019).
31. Barayeu, U. et al. Hydropersulfides inhibit lipid peroxidation and ferroptosis by scavenging radicals. *Nat. Chem. Biol.* **19**, 28–37 (2023).
32. Wu, Z. et al. Hydropersulfides inhibit lipid peroxidation and protect cells from ferroptosis. *J. Am. Chem. Soc.* **144**, 15825–15837 (2022).
33. Lachmann, A. et al. Massive mining of publicly available RNA-seq data from human and mouse. *Nat. Commun.* **9**, 1366 (2018).
34. Zou, Y. et al. Plasticity of ether lipids promotes ferroptosis susceptibility and evasion. *Nature* **585**, 603–608 (2020).
35. Magtanong, L. et al. Context-dependent regulation of ferroptosis sensitivity. *Cell Chem. Biol.* **29**, 1409–1418 (2022).
36. Abedini, A. et al. Single-cell multi-omic and spatial profiling of human kidneys implicates the fibrotic microenvironment in kidney disease progression. *Nat. Genet.* **56**, 1712–1724 (2024).
37. Tsherniak, A. et al. Defining a cancer dependency map. *Cell* **170**, 564–576 (2017).
38. Anastasilakis, A. D. et al. Lipid profile after pharmacologic discontinuation and restoration of menstruation in women with endometriosis: a 12-month observational prospective study. *J. Clin. Med.* **12**, 5430 (2023).
39. Li, J. L., Okada, S., Hamazaki, S., Deng, I. L. & Midorikawa, O. Sex differences in ferric nitrilotriacetate-induced lipid peroxidation and nephrotoxicity in mice. *Biochim. Biophys. Acta* **963**, 82–87 (1988).
40. Belavgeni, A. et al. Exquisite sensitivity of adrenocortical carcinomas to induction of ferroptosis. *Proc. Natl Acad. Sci. USA* **116**, 22269–22274 (2019).
41. Bordoni, L. et al. Longitudinal tracking of acute kidney injury reveals injury propagation along the nephron. *Nat. Commun.* **14**, 4407 (2023).
42. Sarhan, M., Land, W. G., Tonnus, W., Hugo, C. P. & Linkermann, A. Origin and consequences of necroinflammation. *Physiol. Rev.* **98**, 727–780 (2018).

[1]Division of Nephrology, Department of Internal Medicine 3, University Hospital Carl Gustav Carus at the Technische Universität Dresden, Dresden, Germany. [2]Department of Medicine V, University Medical Centre Mannheim, University of Heidelberg, Mannheim, Germany. [3]Institute of Clinical Chemistry and Laboratory Medicine, University Hospital Carl Gustav Carus at the Technische Universität Dresden, Dresden, Germany. [4]Max Planck Institute of Molecular Cell Biology and Genetics, Dresden, Germany. [5]Chair of Organic Chemistry, Technische Universität Dresden, Dresden, Germany. [6]Division of Redox Regulation, German Cancer Research Center (DKFZ), DKFZ-ZMBH Alliance, Heidelberg, Germany. [7]Faculty of Biosciences, Heidelberg University, Heidelberg, Germany. [8]Center of Membrane Biochemistry and Lipid Research, University Hospital and Faculty of Medicine Carl Gustav Carus, Technische Universität Dresden, Dresden, Germany. [9]Department of Chemistry and Biomolecular Sciences, University of Ottawa, Ottawa, Ontario, Canada. [10]Equipe Labellisée Ligue Contre le Cancer, Institut Curie, CNRS, INSERM, PSL Research University, Paris, France. [11]Division of Tumor Metabolism and Microenvironment, German Cancer Research Center (DKFZ), Heidelberg, Germany. [12]Institute of Physiology, Christian-Albrecht-University Kiel,

Kiel, Germany. [13]Max Planck Institute for Polymer Research, Mainz, Germany. [14]Service of Rheumatology, Department of Musculoskeletal Medicine, Centre Hospitalier Universitaire Vaudois, University of Lausanne, Lausanne, Switzerland. [15]Clinic for Urology, University Hospital Carl Gustav Carus at the Technische Universität Dresden, Dresden, Germany. [16]Laboratories of Reproductive and Developmental Toxicology, NIEHS, National Institutes of Health, Research Triangle Park, NC, USA. [17]Renal Division, Montefiore Medical Center, Albert Einstein College of Medicine, New York, NY, USA. [18]Institute of Pathology, University Hospital of Cologne, Cologne, Germany. [19]Division for Nephrology, University of Michigan Medical Center, Ann Arbor, MI, USA. [20]Institute of Metabolism and Cell Death, Helmholtz Zentrum München, Neuherberg, Germany. [21]Chair for Molecular Animal Breeding and Biotechnology, Gene Center and Department of Veterinary Sciences, LMU Munich, Munich, Germany. [22]Center for Innovative Medical Models (CiMM), LMU Munich, Oberschleißheim, Germany. [23]German Center for Diabetes Research (DZD), Neuherberg, Germany. [24]Department of Internal Medicine 3, University Hospital Carl Gustav Carus at the Technische Universität Dresden, Dresden, Germany. [25]Diabetes and Nutritional Sciences, King's College London, London, UK. [26]Center for Regenerative Therapies, Technische Universität Dresden, Dresden, Germany. [27]Paul Langerhans Institute Dresden of Helmholtz Centre Munich at University Clinic Carl Gustav Carus of TU Dresden Faculty of Medicine, Dresden, Germany. [28]Division of Nephrology, Department of Medicine, Albert Einstein College of Medicine, New York, NY, USA. [29]These authors contributed equally: Wulf Tonnus, Francesca Maremonti, Shubhangi Gavali. ✉e-mail: andreas.linkermann@medma.uni-heidelberg.de

Methods

Reagents

Chemicals used for cell death assays were dissolved in DMSO. 17β-oestradiol, testosterone and 2-hydroxyoestradiol were dissolved in ethanol. A list of sources of all chemicals is provided in the Supplementary Information.

Cell lines and cell culture

A list of all cell lines used in this study is provided in the Supplementary Information. Human HT1080, HT29, HeLa and mouse NIH-3T3 cell lines were purchased from the American Type Culture Collection, while CD10-135 cells were provided by collaborators. No further validation was initiated. All cell lines underwent regular testing for mycoplasma infection, and all cell lines were grown in a humidified 5% CO_2 atmosphere at 37 °C. HT1080, HT29, HeLa and NIH-3T3 cell lines were cultured in Dulbecco's modified Eagle's medium (DMEM, Thermo Fisher Scientific) supplemented with 10% (v/v) FBS (Thermo Fisher Scientific, 41966029), 100 U ml^{-1} penicillin and 100 µg ml^{-1} streptomycin (Thermo Fisher Scientific, 15140122). CD10-135 cells were cultured in DMEM F-12 Nutrient Mixture with Glutamax (DMEM/F12 Glutamax, Thermo Fisher Scientific, 10565018) supplemented with 10% (v/v) FBS (Thermo Fisher Scientific, 41966029), 100 U ml^{-1} penicillin and 100 µg ml^{-1} streptomycin (Thermo Fisher Scientific, 15140122).

CRISPR–Cas9-mediated gene knockout

Sequences of all guides are provided in the Supplementary Information. The plasmid pSpCas9(BB)-2A-Blast (Addgene, 118055), which contains a blasticidin-resistance gene, was used to insert guide RNAs (gRNAs) targeting various human genes. The plasmid was linearized using BbsI-HF (NEB, R3539L), and gRNAs targeting the human genes *CBS*, *CTH*, *AIFM2*, *ESR1* and *FAR1* were inserted (the sequences are provided in the Supplementary Information). NEB 5-alpha competent *Escherichia coli* (high efficiency, NEB, C2987H) were transformed with plasmids according to the manufacturer's instructions and colonies were grown overnight over LB agar plates (BD Biosciences, 244520) supplemented with 0.1 mg ml^{-1} ampicillin (Roth, 200-708-1) at 37 °C. Single colonies were picked for plasmid propagation and isolation (Macherey-Nagel, 740410.50). To verify plasmid integrity, the isolated plasmids were digested with SacI-HF (NEB, R3156L) and resolved on 1% agarose gel. Transfection was performed using the Neon NxT electroporation system (Thermo Fisher Scientific, NEON1SK), with the electroporation conditions set at 3 pulses of 10 ms at 1,650 V.

HT29 cells were electroporated with plasmids carrying gRNAs targeting *CBS*, *CTH*, *AIFM2* and *ESR1*. Selection was initiated 24 h after transfection using 40 µg ml^{-1} blasticidin (Invivogen, ant-bl-05) and maintained for 2 weeks. Similarly, HT1080 and CD10 cells were electroporated with plasmids containing gRNAs targeting *FAR1*, followed by selection with 20 µg ml^{-1} and 40 µg ml^{-1} blasticidin, respectively, starting 24 h after transfection for 2 weeks. Knockout efficiency was verified by western blot in polyclonal cell populations. The guide sequences are provided in the Supplementary Information.

Plating and treatment of cells

Detachment of HT1080, HT29, HeLa, NIH-3T3 and CD10 cells was performed using trypsin-EDTA (Gibco, 25200056). Cells were then washed twice and seeded in six-well plates (Sarstedt, 83.3920). All cells were seeded at 1×10^5 cells per well in six-well plates. Before the treatment, the medium was changed. Experiments were performed in a total volume of 1 ml.

Cell death assays

Ferroptosis was induced using established FINs: type I FIN, erastin (Sigma-Aldrich); type II FIN, RSL3 (Selleckchem); type III FIN, FIN56 (Sigma-Aldrich); and type IV FIN, FINO2 (Cayman Chemical). Necrosis was additionally induced as previously described by the thioredoxin reductase inhibitor FTC[30]. Unless otherwise indicated, we used 5 µM erastin, 1.13 µM RSL3, 10 µM FIN56, 10 µM $FINO_2$ and 10 µM FTC. After the indicated timepoints, cells were collected and prepared for flow cytometry or western blotting.

Flow cytometry

Cells were collected and the pellets were washed twice in PBS and stained with 5 µl of 7-AAD (BD Biosciences) and 5 µl of annexin-V–FITC (BD Biosciences) added to 100 µl annexin-V binding buffer solution (BD Biosciences). After 15 min, cells were recorded either on the Fortessa LSRII system with the FACS Diva 6.1.1 software (BD Biosciences), or on the Symphony A3 system with the FAVS Diva v9.0 software (BD Biosciences) and subsequently analysed with the FlowJo v.10 software (Tree Star). The flow cytometry procedure was supported by the Flow Cytometry Core Facility of the CMCB Technology Platform at Technical University of Dresden (TU Dresden) and the FACS Facility of the Institute for Physiological Chemistry (TU Dresden).

Western blotting

Cells were lysed in ice-cold 50 mM Tris-HCl, pH 7.5, 150 mM NaCl, 1% NP-40, 5 mM EDTA supplemented with PhosSTOP (Merck), cOmplete (Merck) and 1 mM phenylmethylsulfonyl fluoride for 30 min on ice. Insoluble material was removed by centrifugation (14,000*g*, 30 min, 4 °C). The protein concentration was determined using a commercial BCA assay kit according to the manufacturer's instructions (Thermo Fisher Scientific). Equal amounts of protein (typically 25 µg per lane) were resolved on a 4–15% gradient SDS–PAGE gel and transferred to a PVDF membrane (Bio-Rad). After blocking for 1 h at room temperature, incubation with primary antibody was performed at 4 °C overnight. Primary antibodies ACSL4 (Abcam, ab155282), GPX4 (Abcam, ab125066), CBS (Thermo Fisher Scientific, MA5-17273), CSE (Proteintech, 60234-1-Ig), POR (Abcam, ab180597), ETHE1 (GeneTex, GTX115707) and SQR (Abcam, ab71978) were diluted 1:1,000 in 5% BSA (Serva, 9048-46-8). Primary antibodies PRX (Abcam, ab184868), AGPS (Invitrogen, A115277), FAR1 (Novus Biological, A107209), FSP1 (provided by M. Conrad, 14D7, or Santa Cruz Biotechnology, sc-377120) and β-actin (Cell Signaling, 3700S) were diluted 1:1,000 in low-fat milk (Roth, 68514-61-4). Secondary antibodies, anti-mouse HRP-linked antibody (Cell Signaling, 7076S) and anti-rabbit HRP-linked antibody (Cell Signaling, 7074S), were applied at concentrations of 1:5,000. Proteins were then visualized by enhanced chemiluminescence (ECL, Amersham Biosciences).

Western blot analysis of renal tubules

For western blot analysis of kidney tubules, freshly isolated tubules are transferred into a 2 ml reaction tube. Depending on the pellet size, an approximate volume of 7 to 30 µl of Roti Load 1 (Roth, K929.1) is added, mixed thoroughly and subsequently snap-frozen in liquid nitrogen. The samples were then either stored at −80 °C or used directly for the western blot analysis. It is essential to assess the protein loading equivalency, as a classical Bradford assay cannot be conducted. Between 3 and 7 µl of tubules, contingent on the quantity, was loaded onto the gel. Next, Ponceau staining was performed to evaluate the uniformity of protein loading. If the staining results were consistent, the protocol proceeded as previously outlined for cell samples.

Isolation of primary mouse renal tubules

Primary mouse renal tubules were isolated strictly following a recently published protocol[43]. In detail, mouse kidneys were removed, washed with PBS, decapsualized and sliced in four to five slices. Kidney slices of each kidney were transferred into a 2 ml reaction tube containing 2 mg ml^{-1} collagenase type II in incubation solution (48 µg ml^{-1} trypsin inhibitor, 25 µg ml^{-1} DNase I, 140 mM NaCl, 0.4 mM KH_2PO_4, 1.6 mM $K_2HPO_4 \cdot 3H_2O$, 1 mM $MgSO_4 \cdot 7H_2O$, 10 mM $CH_3COONa \cdot 3H_2O$, 1 mM

a-ketoglutarate and 1.3 mM Ca-gluconate) and digested for 5 min at 37 °C, 850 rpm. Owing to the presence of damaged tubules, the first resulting supernatant was discarded and 1 ml of incubation solution was added to the kidney slices and digested for 5 min at 37 °C, 850 rpm. The supernatant was collected and transferred in a 2 ml reaction tube containing 1 ml ice-cold sorting solution (0.5 mg ml^{-1} bovine albumin in incubation solution). The reaction tubes were left on ice for the tubules to precipitate. The supernatant was removed and the tubules were washed twice with ice-cold incubation solution. Once the tubules precipitated, the supernatant was removed and ice-cold sorting solution was added (the volume was adjusted depending on the number of samples needed for the experiment). Tubules were distributed in a 24-well plate containing DMEM F-12 nutrient mixture without glycine and phenol red (DMEM/F12, custom-made medium provided by Cell Culture Technologies), supplemented with 0.01 mg ml^{-1} recombinant human insulin, 5.5 µg ml^{-1} human transferrin, 0.005 µg ml^{-1} sodium selenite (Na_2SeO_3) and 470 µg ml^{-1} linoleic acid (ITS+1, Sigma-Aldrich, I2521), 50 nM hydrocortisone, 100 U ml^{-1} penicillin and 100 µg ml^{-1} streptomycin (Thermo Fisher Scientific).

Investigation of pig kidney tissue

Six-month-old INSC94Y ($n = 1$, male)[44] and non-transgenic littermates ($n = 2$ (male) and $n = 2$ (female)) as well as one 2.5-year-old male INSC94Y transgenic boar and a 3.5-year-old non-transgenic boar were euthanized. The kidneys were immediately explanted and further processed for tubule isolation. All of the experiments were performed according to the German Animal Welfare Act with permission from the responsible authority (Government of Upper Bavaria, ROB-55.2-2532.Vet-02-19-195), according to the ARRIVE guidelines and Directive 2010/63/EU. Investigators were strictly blinded to experimental groups during data acquisition and analysis.

Primary porcine renal tubules were isolated using an identical procedure along with the corresponding solutions and media to those described for mouse tubules. Owing to the larger size of the porcine kidney, multiple 2 ml reaction tubes were used during the isolation process.

Human renal tubules

Human renal tissue for the isolation of renal tubules was obtained from fresh tumour nephrectomy specimens at the University Hospital Dresden. Informed consent was obtained from all patients; ethical approval was granted through the uro-oncological biobanking agreement. All aspects of the declaration of Helsinki were met. After open nephrectomy, tissue was immediately obtained from a non-tumour-infiltrated area. Appropriate sections of the kidney medulla, lacking tumour tissue, were excised from the kidneys by medical professionals. The sections were stored in 50 ml reaction tubes in PBS until they could be sliced into thin sections in the laboratory, following the same protocol used for mouse and porcine tubules. Owing to the size of the sections, up to ten 2 ml tubes were used. The remainder of the protocol was consistent with that used for the isolation of porcine and murine tubules; however, the incubation times for digestion and precipitation were extended to 10 min due to the higher density of human tissue composition, which complicates the sectioning process. Approval for use of nephrectomy samples was granted by the ethics commission of the TU Dresden (EK194092004). Informed consent for use of extant tissue for research purposes was obtained before biopsy. Refusal did not affect clinical care. Investigators were strictly blinded to experimental groups during data acquisition and analysis.

Human renal biopsies

For the set of human renal biopsies used in this study, we identified samples of patients who underwent renal indication biopsy for mild-to-medium chronic kidney disease of uncertain aetiology at the University Hospital Dresden from 2022 to 2025 that demonstrated minimal chronic tubular injury due to IgA nephritis. Importantly, no other significant comorbidities were present in these patients except for well-controlled hypertension in some cases. The mean ages of the patients were as follows: male (30.25 years), premenopausal female (32.0 years) and postmenopausal female (62.0 years). Fresh biopsy materials were fixed in 4% normal buffered formalin for at least 24 h before embedding in paraffine. After deparaffinization with xylene and rehydration with graded ethanols, unspecific binding was blocked with 3% BSA in PBS and background sniper (50-823-84, Biocare Medical). Subsequently, the primary antibody was incubated at a concentration of 1:5,000 for AGPS (ab236621, Abcam) followed by anti-rabbit secondary antibody (7074S, Cell Signaling). Bound antibody was visualized with a standard polymer horseradish peroxidase system and counterstained with haematoxylin. Stained sections were analysed using the Axio Imager microscope (Zeiss) or Zeiss Observer Z.1 at ×100, ×200 and ×400 magnification. Micrographs were digitalized using an AxioCam MRm Rev. 3 FireWire camera and AxioVision v.4.5 software (Zeiss), or using an AxioCam MRc and Zen 2012 Software (Zeiss), respectively. Semiquantative scoring of the immunohistochemistry staining intensity (ranging from 0 to 3) in the brush border compartment of proximal tubules was performed by an experienced nephropathologist in a strictly double-blinded manner. Approval for use of human renal biopsies was granted by the ethics commission of the TU Dresden (EK 148052012 and BOK-EK-431102023). Informed consent for use of extant tissue for research purposes was obtained before biopsy. Refusal did not affect clinical care. Investigators were strictly blinded to experimental groups during data acquisition and analysis.

Human renal gene expression data

We explored the MetMap500 database through the DepMap portal[45] (https://depmap.org/metmap/vis-app/index.html; last accessed 1 April 2025) and identified 11 $ESR1^+$ as well as 12 $ESR1^-$ breast cancer cell lines. As all ESR-negative cell lines were also negative for HER2, only $ESR1^+HER2^-$ and $ESR1^-HER2^-$ cell lines (7 versus 12) were compared directly. To this end, batch-corrected expression data (Public 24Q4, https://doi.org/10.25452/figshare.plus.27993248.v1) were plotted through the DepMap data explorer 2.0 tool of the Broad Institute[37]. These data were also visualized as a correlation heat map using the same tool.

To compare gene expression data in healthy individuals and patients with AKI, we used an approach published previously of merging scRNA data from KPMP and the Human Kidney Single Cell Transcriptome[36]. These data were analysed using a tool publicly provided by the Suztak Laboratory (https://susztaklab.com/hk_genemap_kpmp/scRNA; last accessed 2 April 2025).

Assessment of tubular necrosis and treatments of murine renal tubules

All experiments included a negative control to assess LDH release at 0 h. No more than 10% LDH release in these negative controls was tolerated as a quality control. Freshly isolated mouse renal tubules were placed in 24-well plates in DMEM/F12 nutrient mixture without glycine and phenol red (DMEM/F12, custom-made medium provided by Cell Culture Technologies), supplemented with 0.01 mg ml^{-1} recombinant human insulin, 5.5 µg ml^{-1} human transferrin, 0.005 µg ml^{-1} Na_2SeO_3 and 470 µg ml^{-1} linoleic acid (ITS + 1, Sigma-Aldrich, I2521), 50 nM hydrocortisone, 100 U ml^{-1} penicillin, and 100 µg ml^{-1} streptomycin (Thermo Fisher Scientific). After the indicated times, the medium of each well was collected and tubules were prepared for an LDH-release assay (see the 'LDH-release assay' section for further details).

In the case of treatment of tubules, the medium or each well of a 24-well plate was incubated with the compounds of interest. Tubules

were added to each well and the samples were prepared for the LDH-release assay.

LDH-release assay

The LDH release of cells or of freshly isolated kidney tubules was measured according to manufacturers' instructions at the indicated timepoints. In brief, an aliquot of the supernatant was taken to assess the experimental LDH values. Subsequently, lysis solution was added for 45 min to induce maximal LDH release before another aliquot of the supernatant was taken. The supernatants were then incubated with CytoTox 96 Reagent for 15 min protected from the light at room temperature before adding stop solution.

Absorbance was measured at 490 nm and calculated as $100 \times \frac{\text{experimental LDH release}}{\text{max LDH release}}$.

Time-lapse imaging

Videos of freshly isolated mouse tubules stained with 50 nM SYTOX Green nucleic acid stain (Life Technologies) in the presence or absence of 150 nM Biotracker 609 Red Ca^{2+} AM dye (Merck Millipore, 5.04297.0001) or 200 nM MitoTracker Red FM (Invitrogen, M22425) were obtained using an oil-immersion ×63/0.3 EC Plan Neofluar objective. For these experiments, high-quality plastic-bottom slides (Ibidi 15 µ-slide 8-well, 80826) were used. The comparison of male and female mouse tubules was performed using a ×2.5/0.3 EC Plan Neofluar objective, while the tubules were plated in a custom-made 3D chamber. An Axiovert 200M or a Zeiss Observer Z.1, both equipped with a large incubation chamber (37 °C), 5% CO_2 and humidity control were used for all of the live imaging experiments. Transmitted light and fluorescence images (GFP BP filter cube, RFP double filter cube) were acquired using an Orca flash 4.0 camera (Axiovert) or an Axiocam 506 colour (Zeiss Observer Z.1). The live imaging procedure was supported by the Light Microscopy Facility, a Core Facility of the CMCB Technology Platform at Technical University of Dresden (TU Dresden), and the CFCI Core Facility Cellular Imaging (TU Dresden).

Quantification of SYTOX positivity in freshly isolated renal tubules

Isolated renal tubules from male or female mice were incubated in a single 3D-printed well separated by a glass slide, stained with SYTOX green nucleic acid stain. Transmitted light and fluorescence time-lapse images (GFP BP filter cube) were acquired (described in more detail in the 'Time-lapse imaging' section). Every 30 min, the images were assessed for the number of tubules exhibiting more than 90% of SYTOX green positivity. For the quantification of cell death propagation, tubules with less than 90% SYTOX positivity were not counted. Debris was not included in the analysis. The total numbers of male and female tubules were visually counted. Data are presented as the percentage of tubules with equal or more than 90% of SYTOX positivity over time.

Electron microscopy

Mouse tubules were isolated according to the above-mentioned protocol, fixed in 4% buffered paraformaldehyde and then fixed in glutaraldehyde and underwent 1 h of post-fixation/contrasting with osmium tetroxide. The samples were then embedded in Epon resin through graded ethanols and propylene oxide. Blocks were polymerized at 80 °C overnight. Semi-thin sections were stained with methylene blue and azure blue. Thin sections were stained with lead citrate and uranyl acetate. Transmission electron microscopy was performed on the Zeiss Electron Microscope EM 906 (Oberkochem). A Wide-Angle Dual-Speed 2K CCD-Camera TRS 465/14 (Tröndle Restlichtverstärkersysteme) was used for image acquisition in combination with Image SP (Tröndle Restlichtverstärkersysteme) as software. Photoshop 2024 for Macintosh (Adobe) was used for final image preparation.

Inhibited egg phosphatidylcholine liposome co-autoxidations (FENIX 1.0)

RTA only. Egg phosphatidylcholine liposomes (1.02 mM) (prepared as previously described[46]) STY-BODIPY (1.02 µM) and di-*tert*-undecyl hyponitrite (DTUN) (0.203 mM) in chelex-treated phosphate-buffered saline (cPBS) (12 mM phosphate, 150 mM NaCl, pH 7.4) were added to the wells of a Nunc black polypropylene round-bottomed 96-well microplate (295 µl). Using a 1–10 µl multichannel pipette, 5 µl of inhibitor solution in DMSO or vehicle only was then added to afford a final volume of 300 µl (final concentration of 1 mM egg-PC, 1 µM STY-BODIPY, 0.2 mM DTUN and inhibitor varying between 2 and 16 µM). The reaction mixtures were manually mixed using a 100 to 300 µl multichannel pipette (set to 250 µl) and the microplate was inserted into a BioTek H1 Synergy microplate reader equilibrated to 37 °C and vigorously shaken for 1 min followed by a 3.5-min delay. Fluorescence was then recorded (λ_{ex} = 488 nm; λ_{em} = 518 nm; gain = 60) every minute for 6 h. For *co*-extruded samples, egg phosphatidylcholine liposomes (final concentration 1.02 mM) (prepared as described above) and inhibitor solution in DMSO (final concentration varied between 2.05 and 16.37 µM) were added to cPBS, vortexed and re-extruded through a 100 nm polycarbonate membrane 15 times. This co-extruded mixture (782 µl) was subsequently diluted with STY-BODIPY (80 µM, 10 µl) and DTUN (20 mM, 8 µl) to yield a final volume of 800 µl (final concentration of 1 mM egg-PC, 1 µM STY-BODIPY, 0.2 mM DTUN, inhibitor varying between 2 and 16 µM in microplate well). The final solution was vortexed for 5 s and 300 µl was plated per well (two wells plated per condition) and the fluorescence was recorded on the BioTek H1 Synergy microplate as described above.

RTA + reductant. Egg phosphatidylcholine liposomes (1.02 mM) (prepared as previously described[46]), STY-BODIPY (1.02 µM), inhibitor (4.07 µM) and DTUN (0.203 mM) in cPBS (12 mM phosphate, 150 mM NaCl, pH 7.4) were added to the wells of a Nunc black polypropylene round-bottomed 96-well microplate (295 µl). Using a 1–10 µl multichannel pipette, 5 µl of reductant solution in cPBS or vehicle only was then added to afford a final volume of 300 µl (final concentration of 1 mM egg-PC, 1 µM STY-BODIPY, 4 µM inhibitor, 0.2 mM DTUN and reductant concentration varies between 4 µM and 100 µM). The reaction mixtures were manually mixed using a 100–300 µl multichannel pipette (set to 250 µl) and the microplate was inserted into a BioTek H1 Synergy microplate reader equilibrated to 37 °C and vigorously shaken for 1 min followed by a 3.5 min delay. The fluorescence was then recorded (λ_{ex} = 488 nm; λ_{em} = 518 nm; gain = 60) every minute for 15 h.

RTA + mFSP1. Egg phosphatidylcholine liposomes (1.03 mM) (prepared as previously described[46]), STY-BODIPY (1.03 µM), inhibitor (4.14 µM), mFSP1 (16.55 nM) and FAD (331 nM) in pH 7.4 TBS buffer were added to the wells of a Nunc black polypropylene round-bottomed 96-well microplate (290 µl). Using a 1–10 µl multichannel pipette, 5 µl of NADPH solution in TBS or vehicle only was then added followed by 5 µl of DTUN solution (12 mM) in ethanol to give a final volume of 300 µl (final concentration of 1 mM egg-PC, 1 µM STY-BODIPY, 4 µM inhibitor, 16 nM mFSP1, 320 nM FAD, 0.2 mM DTUN and NADPH varying between 4 and 64 µM). The reaction mixtures were manually mixed using a 100–300 µl multichannel pipette (set to 250 µl) and the microplate was inserted into the BioTek H1 Synergy microplate reader equilibrated to 37 °C and vigorously shaken for 1 min followed by a 3.5 min delay. Fluorescence was then recorded (λ_{ex} = 488 nm; λ_{em} = 518 nm; gain = 60) every minute for 15 h. For co-extruded samples, egg-phosphatidylcholine liposomes (1.04 mM) and inhibitor in DMSO (4.15 µM) were added to TBS, vortexed and re-extruded through a 100 nm polycarbonate membrane 15 times. This co-extruded mixture (3594 µl) was then diluted with STY-BODIPY (1.74 mM, 2.14 µl), mFSP1 (48.9 µM, 1.22 µl)

and FAD (0.5 mM, 2.38 µl) to achieve a final volume of 3,600 µl of bulk-lipid mixture. Then, 290 µl of bulk-lipid mixture was plated in a Nunc black polypropylene round-bottomed 96-well microplate, followed by 5 µl of NADPH solution in TBS or vehicle. Finally, 5 µl of DTUN solution in ethanol (12 mM) was added (the final concentrations in well were as follows: 1 mM egg-PC, 1 µM STY-BODIPY, 4 µM inhibitor, 16 nM mFSP1, 320 nM FAD, 4–64 µM NADPH and 0.2 mM DTUN). The reaction mixtures were manually mixed and the fluorescence was recorded on the BioTek H1 Synergy microplate as above.

Generation of 5,6,7,8-tetrahydronaphthalene-2,3-diol

To a pressure tube dried overnight at 150 °C in a drying oven was added under inert gas 2,3-dihydroxy-naphthalene (0.162 g, 1.01 mmol, 1.0 eq.), [Rh(cod)Cl]2 (75.0 mg, 0.015 mmol, 1.0 eq., 15 mol%) and polymethylhydrosiloxane (0.18 ml, 3.00 mmol, 3.0 eq.) in methanol (3 ml). The reaction mixture was stirred at room temperature for 2 days. The solvent was removed in a vacuum and the crude product was purified over silica using the running mixture of iso-hexane/ethyl acetate (2.5:1) with addition of 0.2 vol% triethylamine. The product was obtained as an off-white solid (118 mg, 72%). Then, 40 mg of the product was purified by high-performance LC (HPLC) using the running mixture of iso-hexane/ethyl acetate (5:1) and obtained as a colourless solid (8.6 mg, 21%). Rf(isoHex/EA: 3:1) = 0.43 (stained with anisaldehyde); ^{1}H NMR (CDCl3, 300 MHz): δ (ppm) = 6.57 (s, 2H), 4.80 (s, 2H), 2.66–2.61 (m, 4H), 1.76–1.72 (m, 4H)[47].

Measurement of sulfur-containing metabolites by ultra-performance LC–MS

Investigators were strictly blinded to experimental groups during data acquisition and analysis. In brief, the isolated tubules (see the 'Isolation of primary mouse renal tubules' section for the isolation protocol) were washed twice with cold NaCl (0.9%) solution. Subsequently, any excess liquid was carefully removed. To ensure cell lysis and alkylation of thiol and persulfide species, 200 µl of a 5 mM MBB (monobromobimane) solution in 50% methanol was added to the tubules. The samples were then incubated in the dark at room temperature for 20 min. After the incubation period, the tubules were snap-frozen in liquid nitrogen, stored at −80 °C and finally shipped to the designated location on dry ice for further analysis.

The cell suspension was centrifuged at 14,000*g* for 10 min, and 3 µl of supernatant was applied to an Accucore 150 Amide HILIC HPLC column (100 × 2.1 mm, 2.6 µm particle size) equipped with a guard cartridge (at 30 °C). Mobile phase A was 5 mM ammonium acetate in 5% acetonitrile (CH_3CN); mobile phase B was 5 mM ammonium acetate in 95% CH_3CN. The LC gradient program was: 98% B for 1 min, followed by a linear decrease to 40% B within 5 min, then maintain 40% B for 13 min, then return to 98% B in 1 min and finally 5 min at 98% B for column equilibration. The flow rate was 350 µl min^{-1}. The eluent was directed to the electrospray ionization (ESI) source of the Q Exactive (QE) MS from 0.5 min to 19 min after sample injection. Each sample was run with the parallel reaction monitoring (PRM) method for monobromobimane alkylated metabolites. PRM method: scan type: PRM positive mode; runtime: 0.5–10 min. ddMS^2 settings: resolution: 17,500; AGC target: 2×10^5; maximum injection time: 200 ms; loop count: 1; CE: 20, 50 and 80; isolation window: 1.2 *m/z*. For normalization among the samples, the protein pellets were dried on air and then dissolved in 200 µl 100 mM NaOH. The total protein content was determined by performing a BCA assay. PRM data were processed with Skyline[48] (v.21.2.0.425) and normalized to total protein.

LC–MS/MS-based steroid hormone detection

Investigators were strictly blinded to experimental groups during data acquisition and analysis. Kidney tubules were isolated as described above and snap-frozen. To extract the lipophilic components, the tubules were homogenized in a 1.5 ml Eppendorf tube containing 250 µl of isopropanol and 10 µl of internal standard *d*-oestradiol (2,4,16,16-D4, 95-97%, DLM-2487, Cambridge Isotope Laboratories). Then, one-third volume of zirconium beads was added, and the sample was homogenized for 10 min at 4 °C and 300*g* in a TissueLyser II (Qiagen). After that, the sample was centrifuged for 10 min at 13,000*g*. The supernatant was transferred to a new Eppendorf tube, while the beads and pellet were reserved for protein quantification using the BCA Protein Quantification Kit (Pierce BCA Protein Assay Kit, Thermo Fisher Scientific). The supernatant was incubated at −20 °C for 48 h or longer. After incubation, the sample was centrifuged again for 20 min at 4 °C and 13,000*g*, and the supernatant was transferred to another Eppendorf tube and desiccated in a vacuum desiccator.

For lipid extraction, MTBE extraction method was used. Then, 700 µl of a 10:3 mixture of MTBE and methanol (warmed to room temperature) was added to the dried sample. The sample was shaken for 1 h at 4 °C at 1,400 rpm. Then, 140 µl of water was added, and the sample was shaken again for 15 min at 4 °C at 1,400 rpm. The mixture was centrifuged for 15 min at 4 °C at 13,400 rpm. The upper organic phase was collected and transferred to a 1.5 ml Eppendorf tube, where it was evaporated.

For the derivatization with pyridine-3-sulfonyl chloride, 80 µl of sodium bicarbonate buffer (0.1 M, pH 10) and 80 µl of pyridine-3-sulfonyl chloride (2 mg ml^{-1} in acetone) were added to the dried extracts. The mixture was incubated at 60 °C for 15 min under generous shaking. After incubation, the mixture was cooled on ice for 10 min. The samples were centrifuged at 13,500 rpm at 4 °C for 10 min and the supernatant was collected for subsequent MS analysis.

Pyridine sulfonyl derivatives of oestradiol (E2), 2-hydroxyoestradiol (2OH-E2), 4-hydroxyoestradiol (4OH-E2) but also of the internal standard d4-oestradiol (d4-E2) were profiled by LC–tandem MS (LC–MS/MS) using an instrument set-up containing an ultra-performance LC system (Aquity I-class, Waters) coupled to a triple quadrupole linear ion-trap mass spectrometer (QTRAP 6500+, Sciex).

Chromatography separation was achieved using the Kinetex EVO C18 column (150 mm × 2.1 mm, 2.6 µm; Phenomenex) at 40 °C in conjunction with a gradient of aqueous mobile phase A (5 mM ammonium formate) and methanol as mobile phase B. Then, 5 µl of reconstituted samples, kept at 6 °C in the autosampler, were injected into the LC–MS/MS system at a flow rate of 0.350 ml min^{-1} with 57% mobile phase A. At 3.5 min, mobile phase B increased linearly to 46% until 4.0 min, followed by a decrease to 37% until 4.05 min, kept stable until 4.2 min, and then increased to 47.5% at 4.25 min. Next, mobile B was increased linearly to 85% until 9.5 min, then to 100% at 9.80 min. After a hold until 10.30 min, the gradient was returned back to the initial conditions at 10.80 min and was then maintained for another 3.20 min for column equilibration.

Derivatized oestrogens were analysed in multiple-reaction monitoring scan mode (MRM) using positive ESI including the ion source parameters curtain gas (40 psi), ESI voltage (5,500 V), source temperature (500 °C), gas 1 (70 psi) and gas 2 (50 psi). Compound-dependent source and fragmentation parameters were set to 100 V declustering potential, 10 V entrance potential, 45 V collision energy and 10 V cell exit potential.

For detection of E2 und d4-E2 (chromatographic retention time 9.3 min), respective pairs of quantifier and qualifier ions of 414.2–350.2 and 414.2–272.2, and 418.2–354.2 and 418.2–276.2 were used. Isobaric 4OH-E2 and 2OH-E2, baseline separated at retention times of 8.76 min and 8.96 min, respectively, were detected using pairs of 571.2–365.2 and 571.2–79.0.

Data acquisition was performed by Analyst 1.7 (Sciex). Data processing was done by using the Sciex OS-MQ software package. The data were analysed based on the peak area and normalized according to the internal standard and the total protein. For data presentation, the mean of values from the control group (E2 in males) was calculated and other values represented as factor of this mean.

Lipidomics analysis of murine renal tubules

Mouse renal tubules were freshly isolated according to the isolation of primary mouse renal tubules (see above; $n = 6$ for both sexes) and incubated in the presence of vehicle or 30 µM Fer-1 or 10 µM 2OH-E2. At 0 h and 6 h the supernatant was carefully removed, and tubules were subsequently snap-frozen in liquid nitrogen before storage at −80 °C before lipid extraction. Lipids were extracted according to the Folch method as previously described[49]. In brief, SPLASH LIPIDOMIX (Avanti Polar Lipids, 3 µl) and Cer/Sph Mixture I (Avanti Polar Lipids, 3 µl) internal lipid standards were added to each sample, incubated on ice for 15 min followed by the addition of ice-cold methanol (300 µl) and ice-cold chloroform (600 µl). The samples were vortexed and incubated at 4 °C for 1 h on a rotary shaker. Phase separation was induced by addition of ice-cold water (150 µl), followed by vortexing, incubation at 4 °C (10 min) and centrifugation (1,000*g*, 10 min, 4 °C). All extraction solvents contained 1 µg ml^{-1} butylated hydroxytoluene (BHT) to avoid oxidation. The organic phase was collected and dried in a vacuum concentrator.

For LC–MS analysis, lipids were resuspended in 50 µl of isopropanol and centrifuged, and 40 µl was transferred to glass vials. Lipids were separated by reversed-phase chromatography (Accucore C30 column; 150 mm × 2.1 mm 2.6 µM 150 Å, Thermo Fisher Scientific) using a Vanquish Horizon UHPLC system (Thermo Fisher Scientific) coupled on-line to the Orbitrap Exploris 240 mass spectrometer (Thermo Fisher Scientific) equipped with a HESI source. Lipids were separated at a flow rate of 0.3 ml min^{-1} (column temperature 50 °C) using the following gradient: 0–10 min, 30% to 80% B (curve 5); 10–27 min, 80% to 95% (curve 5); 27–31 min, 95% to 100% (curve 5); 31–37 min, isocratic 100% (curve 5); 37–42 min, re-equilibration at 30% B (curve 5). Eluent A consisted of acetonitrile:water (50:50, v/v, both ULC/MS-CC/SFC grade, Biosolve-Chemicals) and eluent B comprised 2-propanol:acetonitrile:water (85:10:5, v/v/v), both containing 5 mM ammonium formate (MS grade, Sigma-Aldrich) and 0.1% formic acid (ULC/MS-CC/SFC grade, Biosolve-Chemicals). Full MS settings were as follows: spray voltage, 3,500 V; sheath gas, 40 arb units; aux gas, 10 arb units; sweep gas, 1 arb unit; ion transfer tube, 300 °C; vaporizer temperature, 370 °C; EASY-IC run-start; default charge state, 1; resolution at *m/z* 200, 120,000; scan range, *m/z* 200–1,200; normalized AGC target, 100%; maximum injection time, auto; RF lens, 35%. Data-dependent acquisition was based on a cycle time (1.3 s) at a resolution of 30,000; isolation window, 1.2 *m/z;* normalized stepped collision energies, 17,27,37%; AGC target, 100%; maximum injection time, 54 ms.

Lipid identification was performed using Lipostar2. Features with isotopic pattern and MS/MS spectrum were matched against the LIPID MAPS database and selected based on automatic approval (3–4 stars). After manual approval based on an established LC–MS/MS lipid-identification strategy[50], lipid identities and chromatographic peak areas were exported and used for further analysis. Peak areas were normalized according to lipid standard abundances of the SPLASH LIPIDOMIX and Cer/Sph Mixture I and protein content of the samples. Normalized peak areas were autoscaled using MetaboAnalyst 5.0. Lipids showing significant changes in abundance (analysis of variance (ANOVA), $P < 0{,}01$) were visualized through heat maps generated in Genesis v.1.8.1 (Bioinformatics TU-Graz). Investigators were strictly blinded to experimental groups during data acquisition and analysis.

Mice

Male and female mice (aged 8–12-week-old) were co-housed 2–5 mice per cage in individually ventilated cages in our facility at the Medizinisch-Theoretisches Zentrum (MTZ) at the Medical Faculty of the Technical University of Dresden (TU Dresden). All wild-type mice (C57BL/6N) were initially provided by Charles River at the age of 6–7 weeks. *Aifm2*$^{-/-}$ mice (*B6.129-Aifm2*^{tm1Marc}*/Ieg*) were described from our laboratory previously[21]. *Gsdmd-Mlkl*-dKO mice (*Mlkl*$^{tm1.2Wsa}$ × *C57BL/6N-Gsdmd*^{em4Fcw}*/J*) were maintained in our facility and were described previously[51]. *Gpx4*$^{fl/fl}$*ROSA26-creERT2* mice were maintained in the Conrad laboratory in Munich as previously described[20]. CTH-deficient mice (*Cth*^{tm1lish}) were described previously[52] and were co-housed with wild-type littermates at groups of 2–5 mice at the Centre Hospitalier Universitaire Vaudois (University of Lausanne). Experiments on CTH-deficient mice were performed on-site in Lausanne as approved by local authorities. *Esr1*-deficient mice (*B6N(Cg)-Esr1*$^{tm4.2Ksk}$*/J*)[53] were purchased from Jackson Laboratories and bred from heterozygous male and female mice.

The genotype was validated by PCR of tail biopsies for all strains. If not otherwise specified, experiments were performed according to German animal protection laws and were approved by ethics committees and local authorities in Dresden (Landesdirektion Sachsen, Germany) or Munich (Germany) as described below.

Induction of *Gpx4* knockout in mice

For survival and end-point studies, the tamoxifen-inducible conditional mouse strain *Gpx4*$^{fl/fl}$*ROSA26-creERT2* was used as previously described[20]. In brief, to induce *Gpx4* deletion, tamoxifen was first dissolved in Miglyol at a concentration of 20 mg ml^{-1} (Tamoxifen, Sigma-Aldrich, T5648-1G; Miglyol, Caelo 3274-250mL), whereupon 100 µl was injected intraperitoneally on days 0 and 2. To detect potential gender-specific differences in survival time, the mice were monitored daily and euthanized by cervical dislocation after presenting with symptoms of acute kidney failure (humane end point). For the end-point study, mice were again injected with tamoxifen twice, and serum and kidneys were collected at day 10. All animals were bred and maintained under standard specific-pathogen free + individually ventilated cage conditions with food and water ab libitum and all studies were approved by the government of Upper Bavaria (Regierung von Oberbayern, Germany: ROB-55.2-2532.Vet_02-20-51).

Bilateral kidney IRI injury model

All male and female mice were strictly matched for weight, age and genetic background. Bilateral kidney IRI was performed as described in detail previously[43]. In essence, 30 min before anaesthesia, mice received a single intraperitoneal dose of a ferrostatin (Fer-1 (10 mg per kg at 200 µl), UAMC-2303 (200 µl 2.5 mM solution in 0.9% NaCl), or 2OH-oestradiol (10 mg per kg, 200 µl) or a corresponding vehicle control as indicated. Then, 15 min before surgery, all mice received 0.1 µg per g body weight buprenorphine-HCl for analgesia. Anaesthesia was induced by the application of 3 l min^{-1} of volatile isoflurane with pure oxygen in the induction chamber of a COMPAC5 (VetEquip) small animal anaesthesia unit. After achieving a sufficient level of narcosis, typically within 2 min, mice were placed in a supine position on a temperature-controlled self-regulated heating system calibrated to 38 °C and fixed with stripes at all extremities. Anaesthesia was reduced to a maintenance dose of 1.5 l min^{-1} isoflurane. Breathing characteristics and levels of analgesia were closely assessed visually. The abdomen was opened layer-by-layer to create a 2 cm wide opening. Blunt retractors (Fine Science Tools (FST)) were placed for convenient access. With the use of a surgical microscope (Carl Zeiss), sharp forceps were used to pinch retroperitoneal holes directly cranially and caudally in the renal pedicles. Using this access, a 100 g pressure micro serrefine (FST, 18055-03) was placed onto each pedicle to induce ischaemia. Time difference between the placement of both serrefines was recorded (typically <40 s, controlled in all cases to under 1:00 min), the gut was returned into the abdominal cavity and the opening was covered with the two gauze pieces. Then, 1 min before ending of target ischaemia time, the renal pedicles were visualized again and clamps removed exactly at the indicated times (1 s tolerance). The parietal peritoneum and the cutis, respectively, were closed separately by continuous seams using a 6-0 monocryl thread (Ethicon). Isoflurane application was stopped

immediately thereafter and 1 ml of prewarmed PBS was administered intraperitoneally to compensate for any possible dehydration during surgery and to control for potential leakiness of the seams. The mice were divided into pairs of two and put back into the cages. 0.1 µg per g buprenorphine-HCl was administered every 8 h for analgesia. After a 48 h observation period, blood was collected by retroorbital puncture and the mice were euthanized by neck dislocation. The right kidney was removed to be fixed for 24 h in 4% normal buffered formalin and transferred to 70% ethanol for storage at room temperature. The left kidney was removed and shock frozen in liquid nitrogen before transfer to −80 °C for storage.

In this study, we applied different doses of ischaemia. For male mice, we defined 36 min as a hard ischaemia dose (Figs. 1a,b and 2j–m and Extended Data Fig. 5g,h). For female mice, three different doses were used from a titration experiment (Extended Data Fig. 1f–i) defining a medium ischaemia dose of 36 min (Figs. 2k–j,n–q and 3p–r and Extended Data Figs. 1b–e, 5i and 8c). A light ischaemia was defined as 30 min, whereas a hard ischaemia was set at 45 min (Figs. 1i–l and 4c–f and Extended Data Figs. 1a and 9a–d). Inhibitors and vehicle solution were freshly prepared and put on ice until use in a blinded manner. UAMC-3203 was applied intraperitoneally 15 min before surgery in 2.5 mM with 0.9% NaCl in a final volume of 200 µl, Fer-1 was applied intraperitoneally 15 min before surgery (5 mg per kg) in a 200 µl final volume and 2OH-E2 (10 mg per kg) in a 200 µl final volume.

To test the effect of ferrostatins in different doses of ischaemia, either vehicle or UAMC-3203 was applied 15 min before surgery as described above to 10-week-old C57BL/6N female wild-type mice. Surgery was performed as described above with ischaemia times escalating from 30 min to 45 min. After 48 h, blood was taken and the kidneys were removed and processed as described above (Supplementary Fig. 2j–l).

All IRI experiments were approved by the government of Saxony (Landesdirektion Sachsen, Germany; TVV 07/2021 and TVV 38/2024).

Ovariectomy

Ovariectomy was performed using an abdominal approach. At 15 min before surgery, all mice received 0.1 µg per g body weight buprenorphine-HCl for analgesia. Anaesthesia was induced by the application of volatile isoflurane with pure oxygen in the induction chamber of the COMPAC5 (VetEquip) small animal anaesthesia unit. After achieving a sufficient level of narcosis, typically within 2 min, mice were placed in a supine position on a temperature-controlled self-regulated heating system calibrated to 38 °C and fixed with stripes at all extremities. Surgical access to the abdominal cavity was created in the lower abdomen and the right ovary was visualized first. After ligation of the blood supply, the ovary was removed; the same procedure was applied to the left ovary. Next, the abdomen was closed layer by layer and the mice were set back into the individually ventilated cage in pairs. Then, 7 days later, IRI surgery was performed as described above partially using the previous abdominal access. Ovariectomies were approved by the government of Saxony (Landesdirektion Sachsen, Germany; TVV 38/2024).

Histology

Organs were dissected as indicated in each experiment and put in 4% (v/v) neutral-buffered formaldehyde, fixated for 24 h and then transferred to 70% ethanol for storage. In general, the kidneys were dehydrated in a graded ethanol series and xylene, and finally embedded in paraffin. Paraffin sections (3–5 µm) were stained with periodic acid–Schiff (PAS) reagent, according to a standard routine protocol. The stained sections were analysed using the Axio Imager microscope (Zeiss) or Zeiss Observer Z.1 at ×100, ×200 and ×400 magnification. Micrographs were digitalized using an AxioCam MRm Rev. 3 FireWire camera and AxioVision v.4.5 software (Zeiss), or using an AxioCam MRc and Zen 2012 Software (Zeiss), respectively. Organ damage was quantified by two experienced pathologists in a double-blinded manner on a scale ranging from 0 (unaffected tissue) to 10 (most severe organ damage). For the scoring system, tissues were stained with PAS, and the degree of morphological involvement in renal failure was determined using light microscopy. The following parameters were chosen as indicative of morphological damage to the kidney after IRI: brush border loss, red blood cell extravasation, tubule dilatation, tubule degeneration, tubule necrosis and tubular cast formation. These parameters were evaluated on a scale of 0–10, which ranged from not present (0), mild (1–4), moderate (5 or 6), severe (7 or 8), to very severe (9 or 10). Each parameter was determined on at least five different animals.

Software for illustrations

Illustrations were created using Affinity Designer 2.6, Affinity Photo 2.6 (Serif), Prism v.10.5.0 and Adobe Illustrator v.26.0.2.

Statistical analysis

Statistical analyses were performed using Prism 10 (GraphPad). For comparisons of single groups, a two-tailed parametric *t*-test with Welch's correction (Figs. 1i–k,m,n, 2g,h,k–m,o–q, 3h,p–r and 4d–f,i and Extended Data Figs. 1b–d, 2b,c, 5f, 8a and 9a–c,k) or a nonparametric Mann–Whitney *t*-test (Fig. 1a,b) was used. For multiple or repeated comparisons, one-way ANOVA (Figs. 2b and 5i,s, Extended Data Figs. 3a–m, 4b–g, 5a,b, 6b,c, 7h,i and 9m and Supplementary Figs. 3a–m and 4b–d) or two-way ANOVA was used (Figs. 1c,h, 2i, 3i,o, 4a and 5g,j, Extended Data Figs. 7c, 8b and 9n and Supplementary Fig. 2d). To test the null hypothesis in the survival experiments, we plotted the animals in a Kaplan–Meier curve and used the log-rank test for statistics (Extended Data Fig. 2d). For dose–response curves, a four-parameter variable slope nonlinear fit model with least-squares regression without weighting was applied. Extra sum-of-squares *F*-tests were used to compare IC_{50} values (Figs. 1f and 3g and Extended Data Figs. 7e–g and 8f,g). For Extended Data Fig. 10i, statistics were derived from https://susztaklab.com/hk_genemap_kpmp/scRNA.

Comparisons were considered to be significant when $P \leq 0.05$. If no significant difference between groups was detected, we did not indicate this specifically. Data were plotted as the mean ± s.d. if not specified otherwise.

All concrete *P* values are provided as Source data.

Reproducibility

All mice were strictly matched for weight, age and genetic background. Mice were selected into groups according to genotype and sex. Otherwise, they were selected randomly. All mouse experiments were conducted in a strictly double-blinded manner during data collection and analysis. Group sizes were planned ahead of experiments as required by German animal welfare regulations under strict application of 3R initiatives. During all of the experiments involving mammal biomaterials (mice, pigs, humans), investigators were blinded to experimental groups during data acquisition and analysis. No blinding was performed for cell culture assays.

Reporting summary

Further information on research design is available in the Nature Portfolio Reporting Summary linked to this article.

Data availability

Source data for lipidomics data have been uploaded to Zenodo[54] (https://doi.org/10.5281/zenodo.15676640). Lipid species were matched against the LIPID MAPS database using Lipostar2. RNA-seq results for $ESR1^+$ and $ESR1^-$ breast cancer cell lines are publicly available through the DepMap portal (https://www.depmap.org/portal), public dataset 24Q4. Human renal gene expression data were obtained by merging scRNA data from KPMP and the Human Kidney Single Cell Transcriptome using a tool publicly provided by the Suztak Lab

(https://susztaklab.com/hk_genemap_kpmp/scRNA). Source data are provided. Uncropped western blots are provided in the Supplementary Information.

Code availability

No specific code was generated or used for this paper.

43. Belavgeni, A., Maremonti, F. & Linkermann, A. Protocol for isolating murine kidney tubules and ex vivo cell death assays. *STAR Protoc.* **5**, 103005 (2024).
44. Renner, S. et al. Permanent neonatal diabetes in *INS*^{C94Y} transgenic pigs. *Diabetes* **62**, 1505–1511 (2013).
45. Jin, X. et al. A metastasis map of human cancer cell lines. *Nature* **588**, 331–336 (2020).
46. Li, B. et al. Besting vitamin E: sidechain substitution is key to the reactivity of naphthyridinol antioxidants in lipid bilayers. *JACS* **135**, 1394–1405 (2013).
47. He, Y., Tang, J., Luo, M. & Zeng, X. Regioselective and chemoselective reduction of naphthols using hydrosilane in methanol: synthesis of the 5,6,7,8-tetrahydronaphthol core. *Org. Lett.* **20**, 4159–4163 (2018).
48. MacLean, B. et al. Skyline: an open source document editor for creating and analyzing targeted proteomics experiments. *Bioinformatics* **26**, 966–968 (2010).
49. Folch, J., Lees, M. & Sloane Stanley, G. H. A simple method for the isolation and purification of total lipides from animal tissues. *J. Biol. Chem.* **226**, 497–509 (1957).
50. Lange, M. et al. AdipoAtlas: a reference lipidome for human white adipose tissue. *Cell Rep. Med.* **2**, 100407 (2021).
51. Tonnus, W. et al. Gasdermin D-deficient mice are hypersensitive to acute kidney injury. *Cell Death Dis.* **13**, 792 (2022).
52. Ishii, I. et al. Cystathionine gamma-lyase-deficient mice require dietary cysteine to protect against acute lethal myopathy and oxidative injury. *J. Biol. Chem.* **285**, 26358–26368 (2010).
53. Hewitt, S. C. et al. Biological and biochemical consequences of global deletion of exon 3 from the ER alpha gene. *FASEB J.* **24**, 4660–4667 (2010).
54. Tonnus, W. et al. Data for 'Multiple estradiol functions inhibit ferroptosis and acute kidney injury'. *Zenodo* https://doi.org/10.5281/zenodo.15676640 (2025).

Acknowledgements We thank A. Pioch, R. Opitz and M. Hoffmann for technical assistance; T. Akaike for providing GSSSG, and R. Sancho for continuous discussions. Work in the Linkermann laboratory was funded by the German Research Foundation SFB-TRR205, SFB-TRR 127, SPP2306 and a Heisenberg professorship to A.L., project number 324141047, and the international research training group (IRTG/GRK) 2251 and 3019. It was further supported by the BMBF (FERROPath consortium), and the DFG-Sachbeihilfe LI 2107/10-1 and the ForTra GmbH für Forschungstransfer. Work was further supported by the TU Dresden/Kings College London transcampus initiative (A.L., W.T., F.M., K.F., M.T., N.B. and J.N.B.). Work in the Conrad laboratory was supported by Deutsche Forschungsgemeinschaft (DFG) (CO 291/7-1, 428858739 and the Priority Program SPP 2306 (CO 291/9-1, 461385412; CO 291/10-1, 461507177)) and PR 1752/3-1 to B. Proneth, the BMBF program FERROPATH (01EJ2205B), and the European Research Council (ERC) under the European Union's Horizon 2020 research and innovation programme (grant agreement no. GA 884754) to M.C.; D.A.P. and M.M. acknowledge the Natural Sciences and Engineering Research Council of Canada for their support (RGPIN-2022-05058). R.R. is supported by the European Research Council under the European Union's Horizon 2020 research and innovation programme (grant agreement no. 647973), Foundation Charles Defforey-Institut de France. Work in the Fedorova laboratory is supported by 'Sonderzuweisung zur Unterstützung profilbestimmender Struktureinheiten 2021' by the SMWK, TG70 by Sächsische Aufbaubank and SMWK; the measure is co-financed with tax funds on the basis of the budget passed by the Saxon state parliament (to M.F.), Deutsche Forschungsgemeinschaft (FE 1236/5-1 to M.F.) and Bundesministerium für Bildung und Forschung (01EJ2205A, FERROPath to M.F.). We also acknowledge the German research foundation for an instrument grant support (INST 269/910-1 FUGG) to M.P. that supported the described project here. U.B. was supported by fellowship of the Japan Society for the Promotion of Sciences (PE23749). Work in the Dick laboratory was funded by the German Research Foundation (DFG; SPP2306, TRR186) and the European Research Council (grant agreement no. 742039).

Author contributions A.L. conceptualized the study and directed the research. W.T., F.M., S.G. and A.L. designed the experiments. W.T. performed mouse studies and acquired human renal materials. W.T., S.G. and L.M.S.G. analysed mRNA data. W.T. and M.N.S. provided tissue stainings including evaluation. K.F., F.M. and A. Belavgeni performed murine tubular experiments and live imaging. N.H. and J.M.W. provided training and technological support on mouse tubules. S.G., F.G. and K.F. generated KO cell lines. S.G., M.N.S., A. Belavgeni, N.L., K.F., N.B., A.H., M.K., A.R., A. Brucker, J.N.B. and M.T. performed cellular ferroptosis assays. S.T., M.P. and A.S. developed a method for the detection of E2 derivatives and performed measurements. D.S., L.S., A.S., U.B. and T.P.D. quantified hydropersulfide species. U.B. provided critical materials. A.H. and B. Plietker synthesized the simplified dihydrobenzene structure. S.P. and M.F. performed and analysed lipidomics. M.M. and D.A.P. performed FENIX assays. C.G. and R.R. evaluated iron-binding capacity. S.N., K.S.K., S.L., B. Proneth and M.C. provided mouse strains. E.W. provided porcine tissue. J.P., C.H. and S.R.B. provided human renal materials. J.U.B. performed electron microscopy. J.N. and L.G. provided critical insights to sex bias in AKI. C.M., K.F. and M.N.S. provided graphical support. A.L. and W.T. wrote the manuscript. All of the authors contributed to data analysis. All of the authors read and critically discussed the manuscript.

Competing interests The authors declare no competing interests.

Additional information

Supplementary information The online version contains supplementary material available at https://doi.org/10.1038/s41586-025-09389-x.

Correspondence and requests for materials should be addressed to Andreas Linkermann.

Peer review information *Nature* thanks Alberto Ortiz and the other, anonymous, reviewer(s) for their contribution to the peer review of this work. Peer reviewer reports are available.

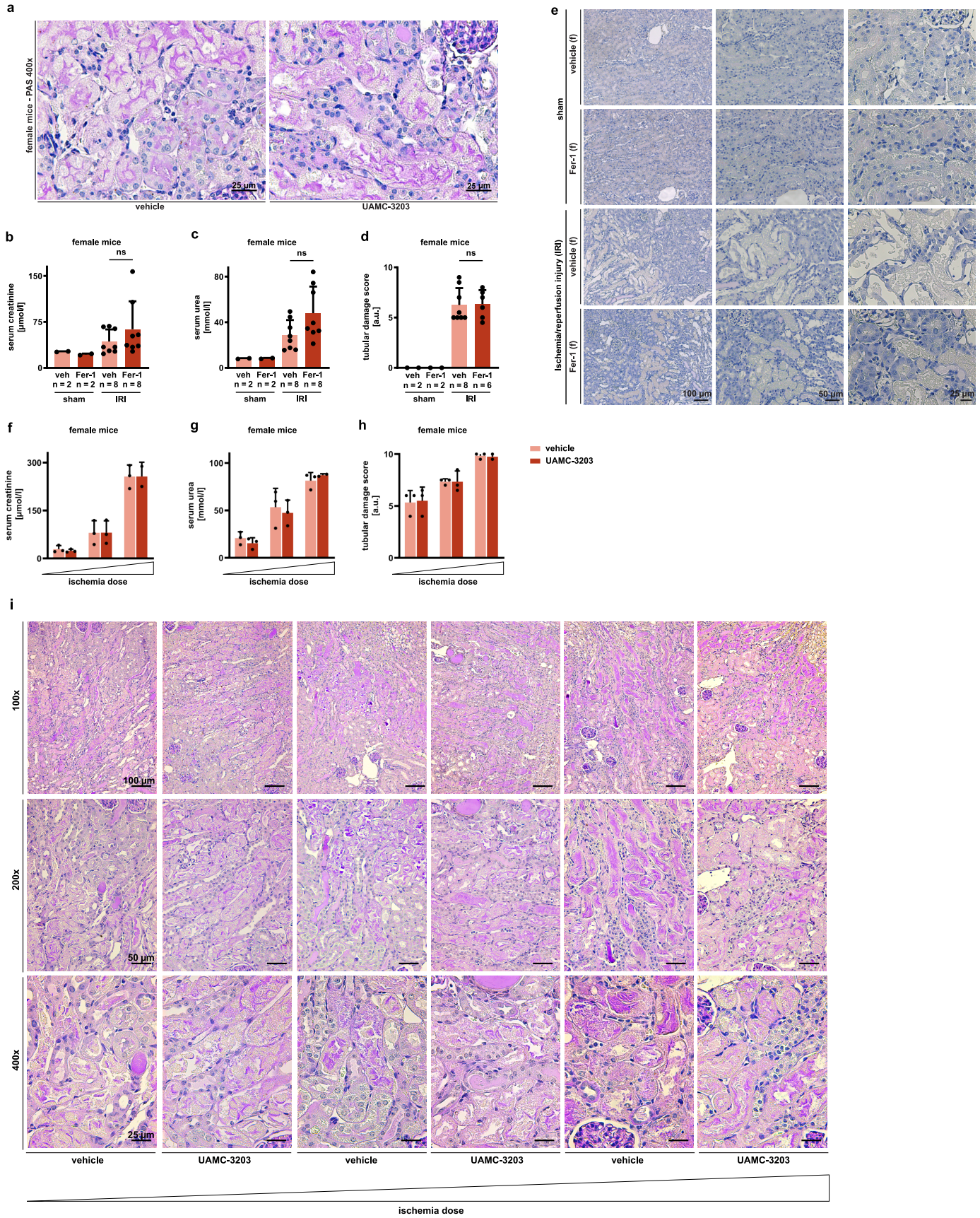

Extended Data Fig. 1 | See next page for caption.

Extended Data Fig. 1 | Abrogated ferroptotic cell death propagation in female renal tubules. (**a**) 400x magnification of tubular injury corresponding to Fig. 1l. 10 mg/kg Fer-1 were applied to female C57Bl/6 mice demonstrating no protective properties regarding (**b**) serum creatinine, (**c**) serum urea, and (**d-e**) tubular injury upon medium ischaemia. (**f-g**) Serum values of creatinine and urea of C57Bl/6 N female wildtype mice upon escalating doses of IRI (mild/medium/hard) treated with either vehicle or UAMC-3203. (**h**) Quantification of tubular injury. (**i**) Representative PAS-stained micrographs of respective groups (n = 3 mice/group).

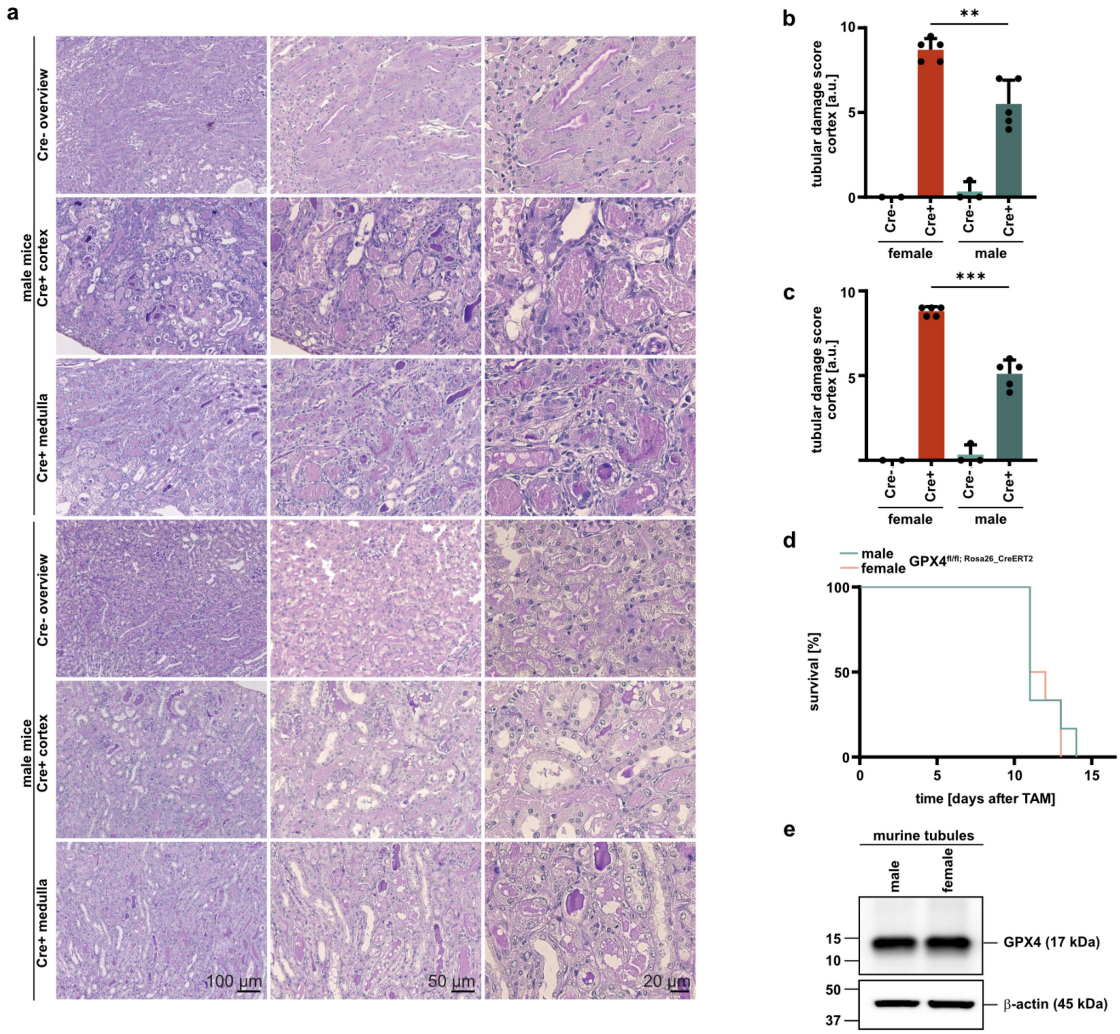

Extended Data Fig. 2 | Sex-specific kidney injury following GPX4 depletion. *Gpx4*$^{fl/fl}$;*ROSA26-CreER*^{T2} transgenic mice were treated with tamoxifen for 10 days. (**a**) PAS staining of renal cortical sections. (**b**) Quantification of tubular injury in the cortex (**c**) and the medulla. (**d**) Despite sex-specific differences in renal injury, no difference in survival times were observed (n = 5 mice/group). (**e**) Western blot demonstrating no difference in tubular GPX4 protein levels in males and females. *$p < 0.05$; **$p < 0.01$; ***$p < 0.001$.

Extended Data Fig. 3 | Estradiol protects against ferroptosis in cell lines. (**a**) Flow cytometry analysis of HT1080 cells simultaneously treated with 17β-E2 (10 µM) and erastin (5 µM), (**b**) FIN56 (10 µM), (**c**) FINO2 (10 µM) or (**d**) ferroptocide (FTC, 10 µM). (**e**) Flow cytometry analysis of NIH-3T3 cells treated simultaneously with 17β-estradiol (10 µM) and erastin (5 µM), (**f**) FIN56 (10 µM), (**g**) FINO2 (10 µM) or (**h**) ferroptocide (FTC, 10 µM). Flow cytometry analysis of CD10 cells treated simultaneously with 17β-estradiol (10 µM) and (**i**) erastin (5 µM), (**j**) RSL3 (1.13 µM), (**k**) FIN56 (10 µM), (**l**) FINO2 (10 µM) or (**m**) ferroptocide (FTC, 10 µM). In all cases, quantification of annexin V / 7-AAD double-negative cells was performed (n = 3 biological replicates). Fer-1 (1 µM) was used as protection control. *$p < 0.05$; **$p < 0.01$.

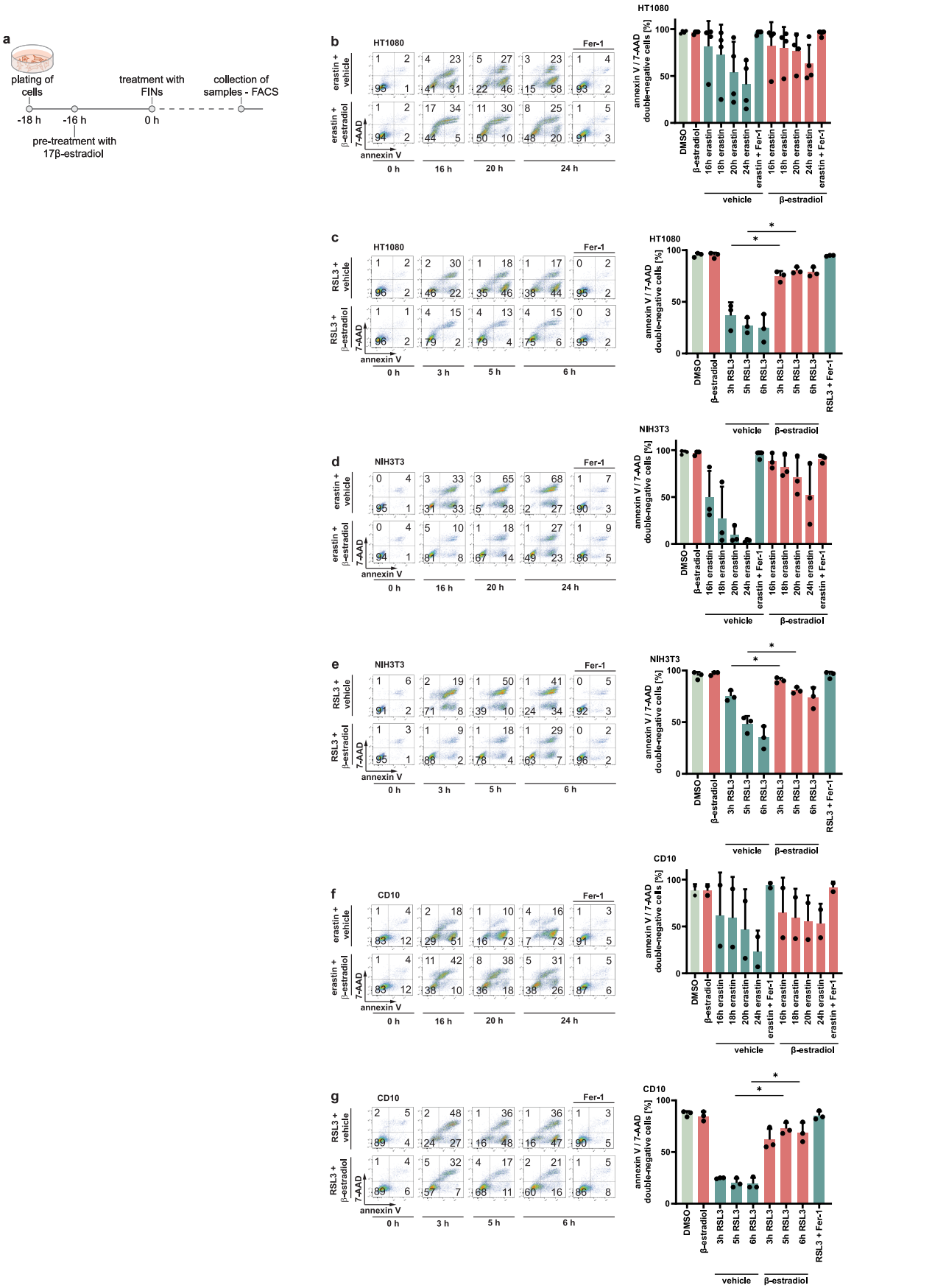

Extended Data Fig. 4 | See next page for caption.

Extended Data Fig. 4 | Estradiol pretreatment protects against ferroptosis. (**a**) Schematic visualization of the experimental setup. Cells were pretreated with 10 μM 17β-estradiol for 16 h before inducing ferroptosis by addition of 5 μM erastin or 1.13 μM RSL3. Flow cytometry was performed at indicated time points and the proportion of annexin V / 7-AAD double-negative cells quantified. E2 protected HT1080 cells long-lasting against (**b**) erastin (n = 5 biological replicates) and (**c**) RSL3 (n = 3 biological replicates). E2 protected NIH3T3 cells long-lasting against (**d**) erastin and (**e**) RSL3 (n = 3 biological replicates). E2 protected CD10 cells long-lasting against (**f**) erastin and (**g**) RSL3 (n = 3 biological replicates). Fer-1 (1 μM) was used as protection control. *$p < 0.05$.

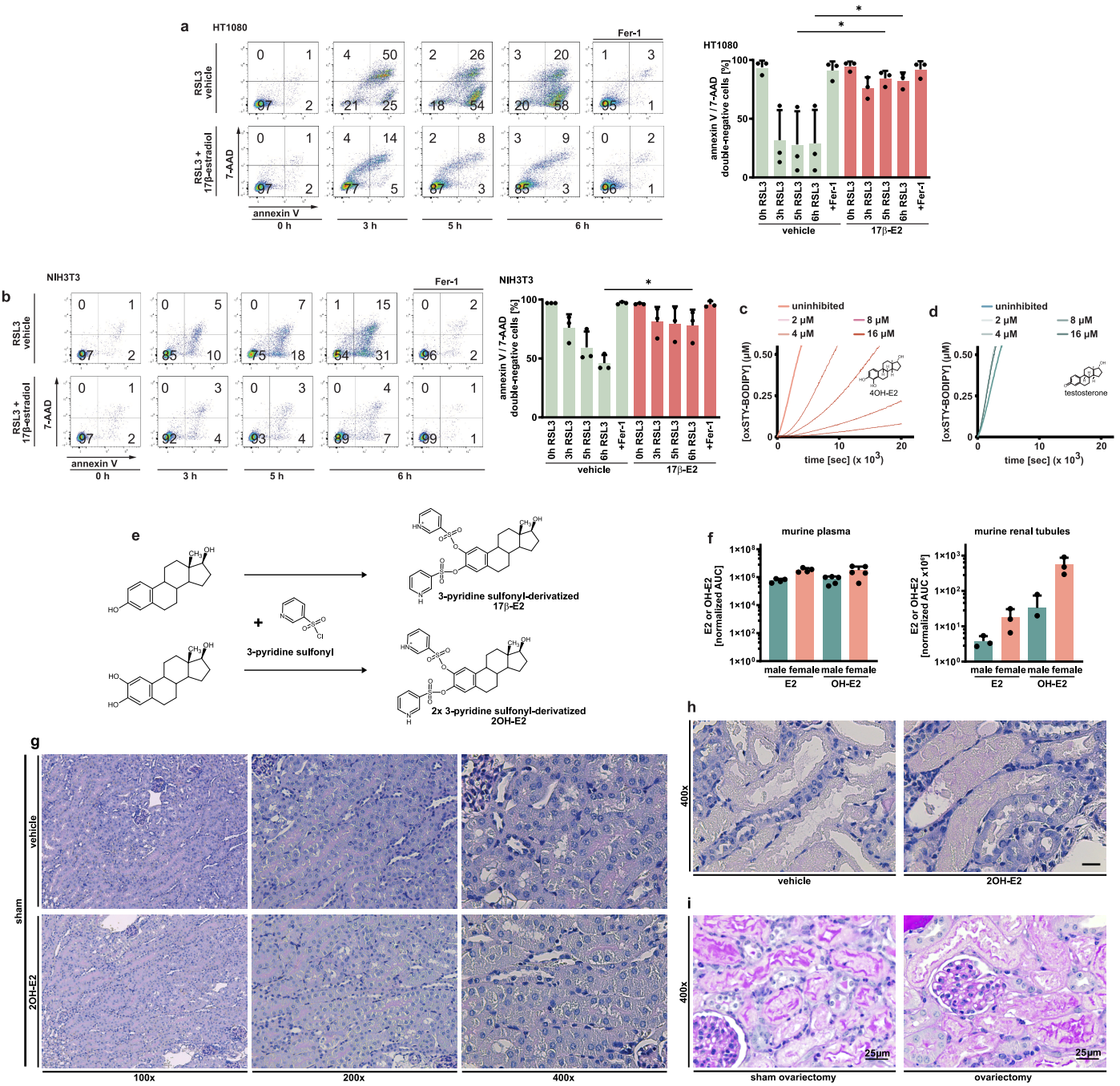

Extended Data Fig. 5 | Oestrogens protect against ferroptosis. (**a**) Flow cytometry analysis of HT1080 and (**b**) NIH3T3 cells simultaneously treated with RSL3 (1.13 µM) and 17β-estradiol (10 µM) for indicated time points. Fer-1 (1 µM) serves as a protection control. The proportion of annexin V / 7-AAD double-negative cells was quantified (n = 3 biological replicates). (**c**) FENIX assays demonstrate radical trapping properties of 4OH-E2, (**d**) but not testosterone (representative of n = 3 biological replicates). (**e**) Strategy of derivatization of 17β-E2 and 2OH-E2 with 3-pyridine sulfonyl. (**f**) Absolute measures of E2 and OH-E2 in plasma (n = 5 mice/sex) and murine renal tubules (n = 3 mice/sex) corresponding to logarithmic transformed data shown in Fig. 2g,h. Normalization to internal standard and protein content was performed. (**g**) Representative micrographs of kidneys of male mice treated with either vehicle or 10 mg/kg 2OH-E2 before sham surgery. (**h**) Representative micrographs in 400x magnification of tubular injury in male mice treated with either vehicle or 2OH-E2 before IRI. (**i**) Representative micrographs (400x) of kidneys after IRI in female mice 7 days after either sham surgery or ovariectomy. $^{*}p < 0.05$.

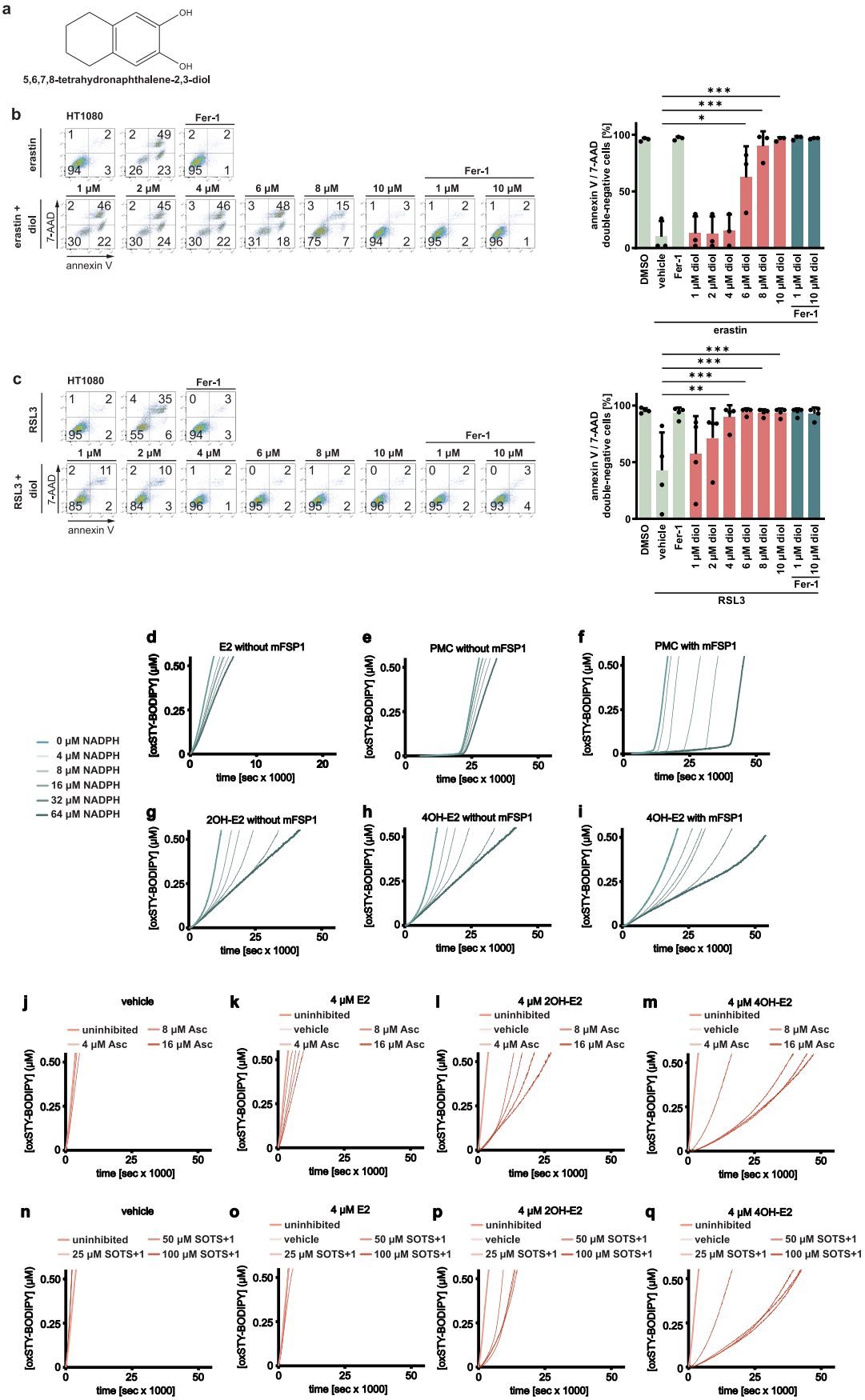

Extended Data Fig. 6 | See next page for caption.

Extended Data Fig. 6 | Estradiol derivatives are recycled to protect against ferroptosis. (**a**) Chemical structure of 5,6,7,8-tetrahydronaphthalene-2,3-diol. (**b**) Flow cytometry analysis of HT1080 cells treated with different concentrations of diol (abbreviation of 5,6,7,8-tetrahydronaphthalene-2,3-diol) and co-treated with erastin (5 μM) (n = 3 biological replicates). (**c**) Flow cytometry analysis of HT1080 cells treated with different concentrations of diol and cotreated with RSL3 (1.13 μM) (n = 4 biological replicates). In all cases, proportion of cells double-negative for annexin V / 7-AAD was quantified. Radical trapping activity was assessed by FENIX assays (representatives of n = 3 biological replicates). (**d**) Activity of 17β-E2 was not enhanced by FAD and NADPH only. (**e-f**) Addition of 16 μM recombinant mFSP1 enhanced radical trapping activity of PMC. (**g**) Radical trapping activity of 2OH-E2 was less potent without addition of mFSP1. (**h-i**) mFSP1 enhanced radical trapping activity of 4OH-E2. (**j**) Ascorbate alone failed to achieve radical trapping activity. (**k**) (17β-)E2 radical trapping activity was not enhanced by ascorbate. (**l**) Ascorbate enhanced radical trapping potency of both 2OH-E2 and (**m**) 4OH-E2. (**n**) FENIX assay of superoxide thermal source (SOTS-1) serving as control showing no regenerative capacity in the absence of a compound that can be oxidized. SOTS-1 thermally decomposes to yield two equivalents of superoxide, which is in equilibrium with its conjugate acid hydroperoxyl radical (HOO•). (**o-q**) FENIX assay of SOTS-1 in the presence of (17β-)E2, 2OH-E2, and 4OH-E2.

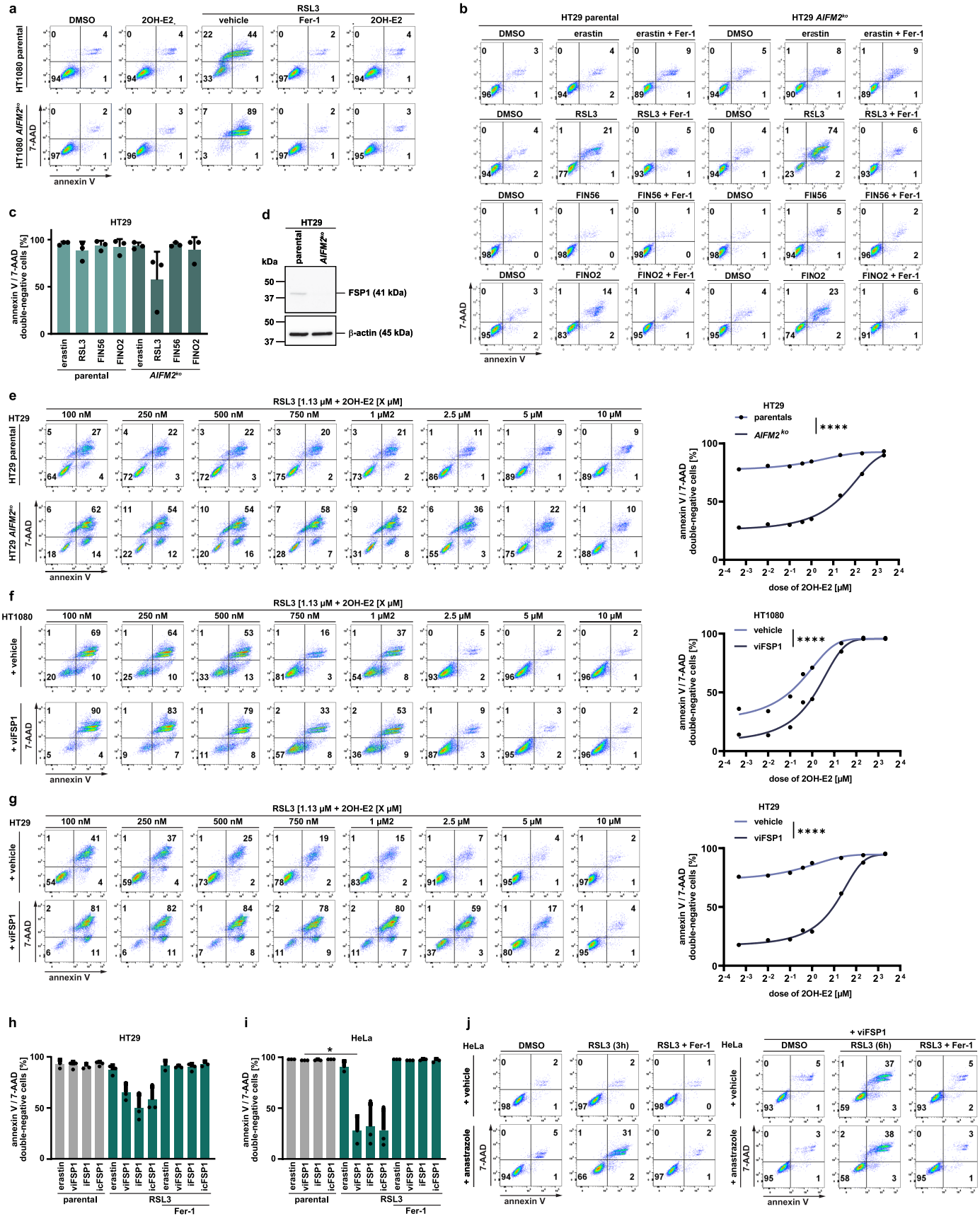

Extended Data Fig. 7 | See next page for caption.

Extended Data Fig. 7 | FSP1 regenerates 2OH-E2 in cellular systems. (**a**) Representative controls corresponding to Fig. 3f (RSL3 1.13 μM; Fer-1 1 μM; 2OH-E2 10 μM). (**b**) FSP1-deficiency sensitizes HT29 cells to RSL3-induced ferroptosis, but not other classes of FINs (erastin 5 μM 24 h; RSL3 1.13 μM 24 h; FIN56 10 μM 48 h; FINO2 10 μM 24 h). (**c**) Quantification of cells double-negative for annexin V / 7-AAD (n = 3 biological replicates). (**d**) Western Blot demonstrating efficacy of AIFM2 knock-out in HT29 cells. (**e**) FSP1-deficiency increased the required dose of 2OH-E2 to protect HT29 cells against RSL3-induced ferroptosis (n = 4 biological replicates). Correspondingly, concomitant treatment with 5 μM viFSP1 increased the required dose of 2OH-E2 to protect both (**f**) HT1080 (n = 4 independent experiments) and (**g**) HT29 cells (n = 3 biological replicates) against RSL3-induced ferroptosis. Various chemical FSP1-inhibitors (5 μM viFSP1, 5 μM icFSP1, or 5 μM iFSP1) sensitized either (**h**) HT29 cells or (**i**) HeLa cells specifically to RSL3-induced ferroptosis (n = 3 biological replicates). (**j**) Inhibition of E2 synthesis in HeLa cells by pretreatment with 5 μM anastrozole for 7 days sensitized to RSL3-induced ferroptosis with no additional effect of viFSP1 (representative of n = 3 biological replicates). $^{*}p < 0.05$; $^{**}p < 0.01$; $^{***}p < 0.001$; $^{****}p < 0.0001$.

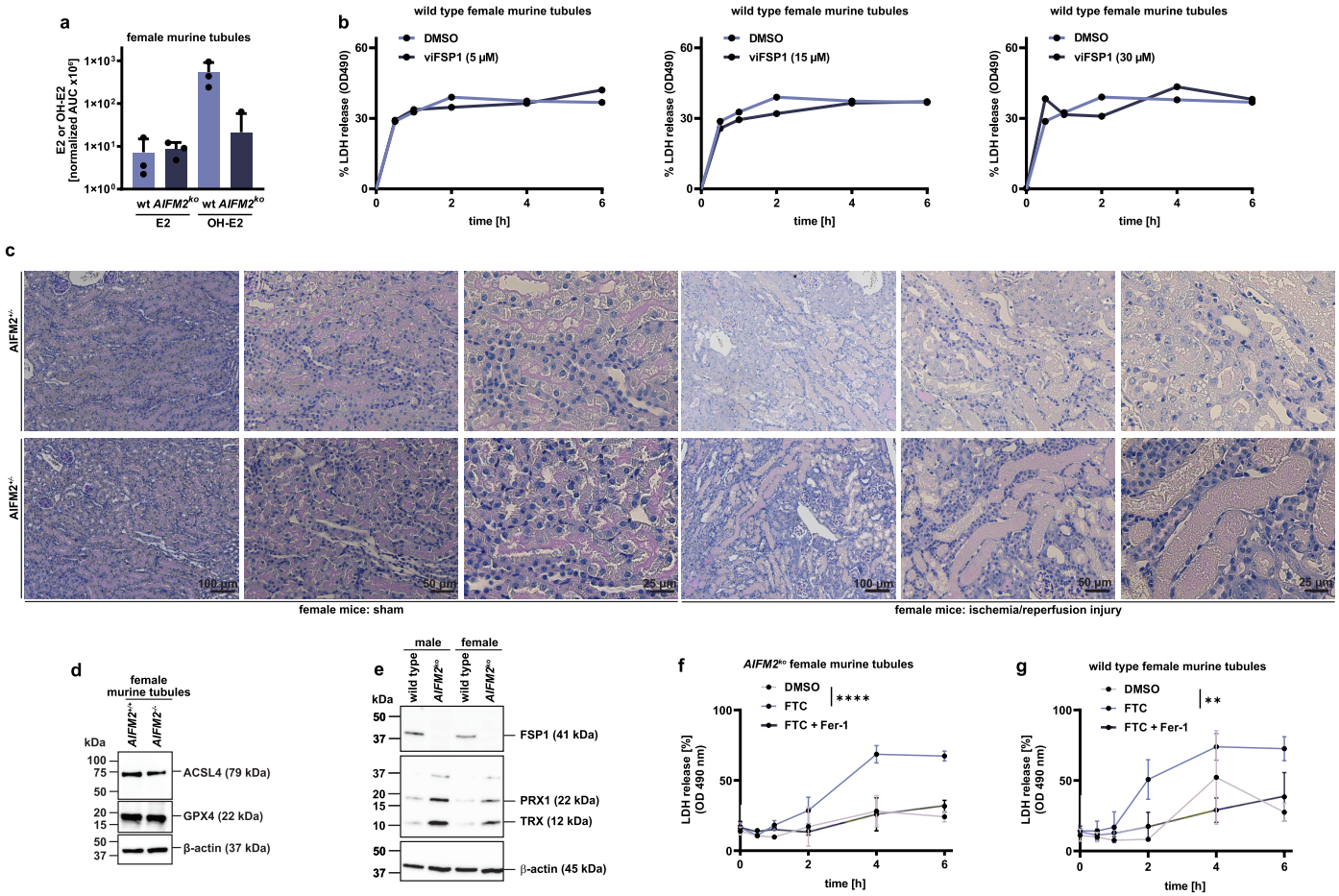

Extended Data Fig. 8 | Impaired FSP1 function does not sensitize female renal tubules to ferroptosis. Logarithmic transformation of measures of E2 and OH-E2 from female murine tubules corresponding to Fig. 3h normalized to internal standard and protein content (n = 3 mice/condition) (**b**) LDH release of female tubules treated with indicated doses of viFSP1 (n = 1 sample/condition) (**c**) Representative micrographs of kidneys from FSP1-deficient female mice or littermates upon either sham surgery or IRI corresponding to Fig. 3p–r. (**d**) Western Blot for GPX4 and ACSL4 from lysates of female tubules comparing littermates and FSP1-deficient mice. (**e**) Western Blot from lysates of isolated kidney tubules incubated with antibodies against the thioredoxin system in response to FSP1 deficiency. (**f-g**) LDH release of female murine tubules treated with the TRX-inhibitor ferroptocide (FTC, 30 µM) demonstrates sensitivity independently of *AIFM2* genotype. Fer-1 (30 µM) served as protection control (n = 3 samples/group) $^{*}p < 0.05$; $^{****}p < 0.0001$.

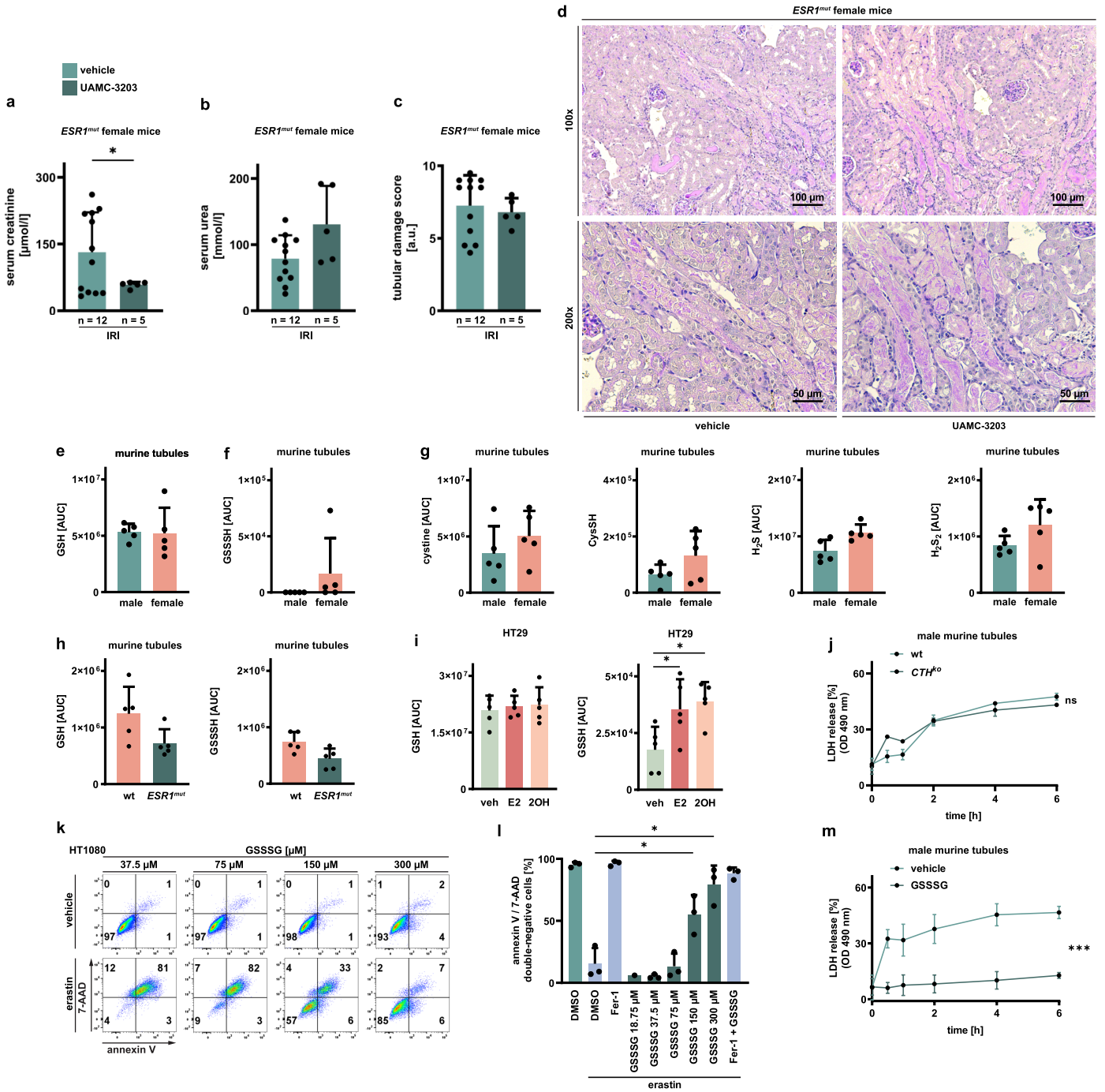

Extended Data Fig. 9 | Effects of ESR1-deficiency on ferroptosis. ESR1-deficient female mice were treated with either vehicle solution or UAMC-3203 upon hard renal IRI (**a-b**). Serum creatinine and urea were measured after 48 h. (**c-d**) Tubular injury was quantified from PAS-stained slides. Levels of (**e**) GSH, (**f**) GSSSH, and (**g**) further sulfur metabolites from lysates of isolated renal tubules of male and female mice (n = 5 samples/group). (**h**) Quantification of GSH and GSSSH from wildtype and ESR1-deficient murine tubules (n = 5 samples/group). (**i**) GSH and GSSH levels in HT29 cells after treatment with 10 µM E2 or 2OH-E2 (n = 5 samples/group). (**j**) LDH release from wild-type and CTH-deficient male murine tubules (n = 2 mice/group). (**k-l**) HT1080 cells were induced to undergo ferroptosis by erastin in the presence of 37.5 µM – 300 µM of GSSSG. Annexin V / 7-AAD double staining was read out by flow cytometry (n = 3 biological replicates) (**m**) LDH release from male wild type tubules treated with vehicle or 300 µM GSSSG (n = 3 samples/group). *$p < 0.05$; **$p < 0.01$; ***$p < 0.001$; ****$p < 0.0001$.

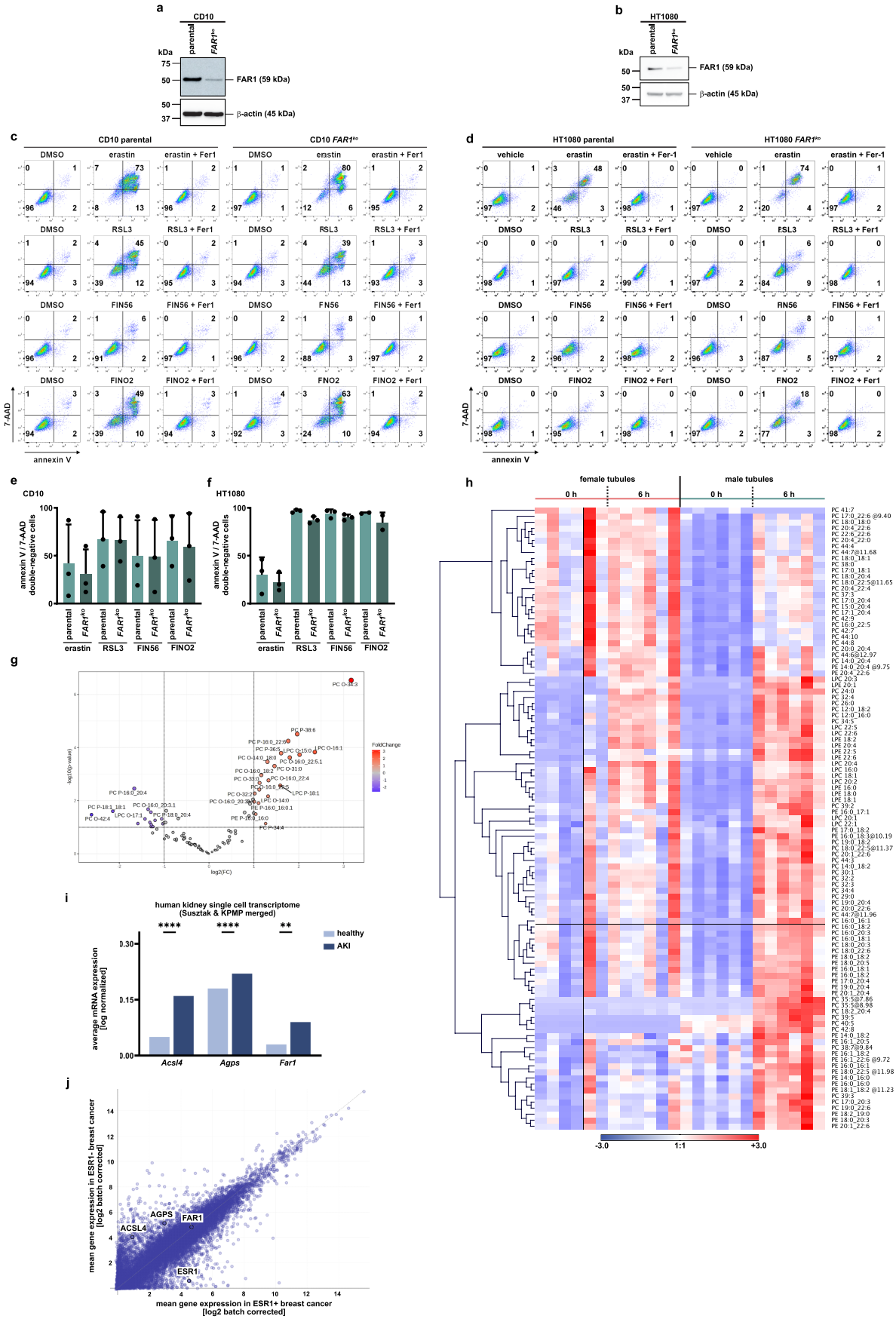

Extended Data Fig. 10 | See next page for caption.

Extended Data Fig. 10 | ESR1 controls ether lipid synthesis. Western Blots demonstrating CRISPR-mediated knock-out of *FAR1* in (**a**) CD10 and (**b**) HT1080 cells. FAR1-deficiency did not sensitize (**c**) CD10 cells or (**d**) HT1080 cells to FINs (5 μM erastin; 1.13 μM RSL3; 10 μM FIN56; or 10 μM FINO2). (**e-f**) quantification of the experiment described in (**c-d**) (n = 3 biological replicates). (**g**) Volcano plot of differential ether lipid abundances in males versus female renal tubules at baseline (0 hr). Tones of red and blue depict lipid species with significantly higher levels in males and females, respectively. (**h**) Heatmap depicting ester lipid plasticity at baseline and following tubular ferroptosis (6 h) in male and female renal tubules (n = 6 samples/sex). (**i**) Average mRNA expression of *Far1*, *Agps*, and *Acsl4*, respectively, in kidney samples of healthy persons and patients with AKI (see Methods). (j) Opposing expression of *Esr1* as well as *Far1*, *Agps*, and *Acsl4* among Her2-negative breast cancer cell lines as determined from the DepMap portal (see Methods). $^{*}p < 0.05$; $^{**}p < 0.01$; $^{***}p < 0.001$; $^{****}p < 0.0001$.

nature portfolio

Corresponding author(s): Prof. Andreas Linkermann

Last updated by author(s): 13.06.2025

Reporting Summary

Nature Portfolio wishes to improve the reproducibility of the work that we publish. This form provides structure for consistency and transparency in reporting. For further information on Nature Portfolio policies, see our Editorial Policies and the Editorial Policy Checklist.

Statistics

For all statistical analyses, confirm that the following items are present in the figure legend, table legend, main text, or Methods section.

n/a	Confirmed
☐	☒ The exact sample size (*n*) for each experimental group/condition, given as a discrete number and unit of measurement
☐	☒ A statement on whether measurements were taken from distinct samples or whether the same sample was measured repeatedly
☐	☒ The statistical test(s) used AND whether they are one- or two-sided *Only common tests should be described solely by name; describe more complex techniques in the Methods section.*
☒	☐ A description of all covariates tested
☐	☒ A description of any assumptions or corrections, such as tests of normality and adjustment for multiple comparisons
☐	☒ A full description of the statistical parameters including central tendency (e.g. means) or other basic estimates (e.g. regression coefficient) AND variation (e.g. standard deviation) or associated estimates of uncertainty (e.g. confidence intervals)
☐	☒ For null hypothesis testing, the test statistic (e.g. *F*, *t*, *r*) with confidence intervals, effect sizes, degrees of freedom and *P* value noted *Give P values as exact values whenever suitable.*
☒	☐ For Bayesian analysis, information on the choice of priors and Markov chain Monte Carlo settings
☒	☐ For hierarchical and complex designs, identification of the appropriate level for tests and full reporting of outcomes
☒	☐ Estimates of effect sizes (e.g. Cohen's *d*, Pearson's *r*), indicating how they were calculated

Our web collection on statistics for biologists contains articles on many of the points above.

Software and code

Policy information about availability of computer code

Data collection

Flow cytometry:
BD Fortessa LSRII using FACS Diva 6.1.1 software
BD Symphony A3 using FACS Diva v9.0 software

Western blot:
Amersham ImageQuant 800

Plate reader:
tecan iControl

Imaging:
Apotome Zeiss Imaging Software
Zeiss AxioVision ver. 4.5 software
Leica Application Suite X
Zeiss Electron Microscope Software

Electron Microscopy:
Zeiss EM 906 Software
ImageSP

FENIX assay:

Agilent BioTek Gen5 v. 3.08.01

LCMS:
Skyline9 (21.2.0.425)
Analyst 1.7 (Sciex)

Lipidomics:
Lipostar2

NMR:
Bruker Topspin 4.1.4 software

Data analysis

Microsoft Excel and PowerPoint, as well as GraphPad Prism 10.2.3 unless stated otherwise

Flow cytometry:
FlowJo software v 10.09.0

Image processing:
Zeiss Zen 3.7
ImageJ 1.53t
Photoshop 2024 for Macintosh

Statistics:
GraphPad Prism 10.2.3

Illustrations:
Adobe Illustrator 2024 28.5.0
Affinity Desginer 2.6.0

LCMS:
Sciex OS-MQ software package

Lipidomics:
MetaboAnalyst 5.0
Genesis 1.8.1

NMR:
MestRenova v.5.0.1-35756
Bruker Topspin 4.1.4 software

For manuscripts utilizing custom algorithms or software that are central to the research but not yet described in published literature, software must be made available to editors and reviewers. We strongly encourage code deposition in a community repository (e.g. GitHub). See the Nature Portfolio guidelines for submitting code & software for further information.

Data

Policy information about availability of data

All manuscripts must include a data availability statement. This statement should provide the following information, where applicable:

- Accession codes, unique identifiers, or web links for publicly available datasets
- A description of any restrictions on data availability
- For clinical datasets or third party data, please ensure that the statement adheres to our policy

Lipidomics data are presented in the Supplementary Tables, lipid species were matched against the LIPID MAPS database using Lipostar2. RNA sequencing results for ESR1+ and ESR1- breast cancer cell lines are publicly available via the DepMap portal (https://www. depmap.org/portal), public dataset 24Q4. Human renal gene expression data were obtained via merging scRNA data from KPMP and the Human Kidney Single Cell Transcriptome via a tool publicly provided by the Suztak Lab (https://susztaklab.com/hk_genemap_kpmp/scRNA). Source Data are provided with this paper. Uncropped Western blots are provided in the Supplementary Information.

Research involving human participants, their data, or biological material

Policy information about studies with human participants or human data. See also policy information about sex, gender (identity/presentation), and sexual orientation and race, ethnicity and racism.

Reporting on sex and gender	Human kidney tissue including both male and female patients were used in this study as thoroughly labelled.
Reporting on race, ethnicity, or other socially relevant groupings	Kidney tissue samples samples were anonymous and no reporting of race, ethnicity or other socially relevant groupings were performed in accordance with German law. The only information revealed were sex, age, and diagnosis.
Population characteristics	Kidney tissue from patients recieving nephrectomy due to renal carcinoma was obtained as anonymous samples. Sex and age of patients was matched to the samples in order to estimate pre- or postmenopausal status. Ages were: 63a (male), 85 a (female), 79a (male), 71a (female)

For patients with IgA nephritis, kidney biopsy samples routinely taken for diagnosis, were selected for low tubular injury and absence of relevant scarring as indicated by the pathologists report (unrelated to this study). Ages were specifically:
Male: 36a, 40a, 24a and 21a
Premenopausal female: 31a, 38a, 25a, and 34a
Postmenopausal female: 74a, 55a, 57a, 62a

Recruitment

Nephrectomy patients were selected upon scheduled standard surgery at the Department of Urology at the University Hospital CGC at the TU Dresden if the surgeon estimated a reasonable amount of healthy adjacent tissue would be available upon nephrectomy. Informed consent was obtained at least 24h previous to surgery. Refusal to participate did not affect clinical care.
Kidney biopsies were routinely taken suscpeted onset of chronic kidney disease at the Department of Nephrology, Medical Clinic and Policlinic 3, University Hospital CGC at the TU Dresden. Informed consent for utilization of extant tissue for research purposes was obtained before biopsy. Refusal did not affect clinical care.

Ethics oversight

Uro-oncological biobanking (Dr. Putz), approved by ethics comittee TU Dresden, Germany for Nephrectomy samples.
Approval for utilization of human renal biopsies was granted by the ethics commission of the TU Dresden (EK 148052012 and BOK-EK-431102023).

Note that full information on the approval of the study protocol must also be provided in the manuscript.

Field-specific reporting

Please select the one below that is the best fit for your research. If you are not sure, read the appropriate sections before making your selection.

☒ Life sciences ☐ Behavioural & social sciences ☐ Ecological, evolutionary & environmental sciences

For a reference copy of the document with all sections, see nature.com/documents/nr-reporting-summary-flat.pdf

Life sciences study design

All studies must disclose on these points even when the disclosure is negative.

Sample size

No sample size calculation was performed, but a minimum of n = 3 chosen for cell biology experiments. For in vivo experiments, mouse cohort groups were at least 5 for those that underwent surgery. No sample size calculation was performed for human samples, and analyses were performed on
availability of these rare samples post-surgery, depending on availability from the patients.

Data exclusions

Technically invalid data (e.g. mice with surgical complications or those that had to be sacrificed before the blood/organ harvesting time points) were excluded from the analysis. Otherwise, no data were excluded.

Replication

Experiments were performed at least three times unless stated otherwise in individual figure legends or methods. Replication was successful and all data are displayed in the manuscript. All replicates of all experiments noted in the captions and/ or the statistical analysis, with data available as source files.

Randomization

Mice were selected into groups according to genotype and sex. Otherwise, they were selected randomly.
For patient samples, they were grouped by sex and age to infer pre or postmenopausal status. Material was available from the hospital and collected in an anonymous fashion for the analysis, other than the indication of sex and age.

Blinding

All in vivo experiments were conducted in a double-blinded manner. Investigators were blinded to group allocation during data collection and analysis for patient samples, LC-MS/MS experiments and lipidomics.

Behavioural & social sciences study design

All studies must disclose on these points even when the disclosure is negative.

Study description

Briefly describe the study type including whether data are quantitative, qualitative, or mixed-methods (e.g. qualitative cross-sectional, quantitative experimental, mixed-methods case study).

Research sample

State the research sample (e.g. Harvard university undergraduates, villagers in rural India) and provide relevant demographic information (e.g. age, sex) and indicate whether the sample is representative. Provide a rationale for the study sample chosen. For studies involving existing datasets, please describe the dataset and source.

Sampling strategy

Describe the sampling procedure (e.g. random, snowball, stratified, convenience). Describe the statistical methods that were used to predetermine sample size OR if no sample-size calculation was performed, describe how sample sizes were chosen and provide a rationale for why these sample sizes are sufficient. For qualitative data, please indicate whether data saturation was considered, and

what criteria were used to decide that no further sampling was needed.

Data collection

Provide details about the data collection procedure, including the instruments or devices used to record the data (e.g. pen and paper, computer, eye tracker, video or audio equipment) whether anyone was present besides the participant(s) and the researcher, and whether the researcher was blind to experimental condition and/or the study hypothesis during data collection.

Timing

Indicate the start and stop dates of data collection. If there is a gap between collection periods, state the dates for each sample cohort.

Data exclusions

If no data were excluded from the analyses, state so OR if data were excluded, provide the exact number of exclusions and the rationale behind them, indicating whether exclusion criteria were pre-established.

Non-participation

State how many participants dropped out/declined participation and the reason(s) given OR provide response rate OR state that no participants dropped out/declined participation.

Randomization

If participants were not allocated into experimental groups, state so OR describe how participants were allocated to groups, and if allocation was not random, describe how covariates were controlled.

Ecological, evolutionary & environmental sciences study design

All studies must disclose on these points even when the disclosure is negative.

Study description

Briefly describe the study. For quantitative data include treatment factors and interactions, design structure (e.g. factorial, nested, hierarchical), nature and number of experimental units and replicates.

Research sample

Describe the research sample (e.g. a group of tagged Passer domesticus, all Stenocereus thurberi within Organ Pipe Cactus National Monument), and provide a rationale for the sample choice. When relevant, describe the organism taxa, source, sex, age range and any manipulations. State what population the sample is meant to represent when applicable. For studies involving existing datasets, describe the data and its source.

Sampling strategy

Note the sampling procedure. Describe the statistical methods that were used to predetermine sample size OR if no sample-size calculation was performed, describe how sample sizes were chosen and provide a rationale for why these sample sizes are sufficient.

Data collection

Describe the data collection procedure, including who recorded the data and how.

Timing and spatial scale

Indicate the start and stop dates of data collection, noting the frequency and periodicity of sampling and providing a rationale for these choices. If there is a gap between collection periods, state the dates for each sample cohort. Specify the spatial scale from which the data are taken

Data exclusions

If no data were excluded from the analyses, state so OR if data were excluded, describe the exclusions and the rationale behind them, indicating whether exclusion criteria were pre-established.

Reproducibility

Describe the measures taken to verify the reproducibility of experimental findings. For each experiment, note whether any attempts to repeat the experiment failed OR state that all attempts to repeat the experiment were successful.

Randomization

Describe how samples/organisms/participants were allocated into groups. If allocation was not random, describe how covariates were controlled. If this is not relevant to your study, explain why.

Blinding

Describe the extent of blinding used during data acquisition and analysis. If blinding was not possible, describe why OR explain why blinding was not relevant to your study.

Did the study involve field work? ☐ Yes ☐ No

Field work, collection and transport

Field conditions

Describe the study conditions for field work, providing relevant parameters (e.g. temperature, rainfall).

Location

State the location of the sampling or experiment, providing relevant parameters (e.g. latitude and longitude, elevation, water depth).

Access & import/export

Describe the efforts you have made to access habitats and to collect and import/export your samples in a responsible manner and in compliance with local, national and international laws, noting any permits that were obtained (give the name of the issuing authority, the date of issue, and any identifying information).

Disturbance

Describe any disturbance caused by the study and how it was minimized.

Reporting for specific materials, systems and methods

We require information from authors about some types of materials, experimental systems and methods used in many studies. Here, indicate whether each material, system or method listed is relevant to your study. If you are not sure if a list item applies to your research, read the appropriate section before selecting a response.

Materials & experimental systems

n/a	Involved in the study
☐	☒ Antibodies
☐	☒ Eukaryotic cell lines
☒	☐ Palaeontology and archaeology
☐	☒ Animals and other organisms
☒	☐ Clinical data
☒	☐ Dual use research of concern
☒	☐ Plants

Methods

n/a	Involved in the study
☒	☐ ChIP-seq
☐	☒ Flow cytometry
☒	☐ MRI-based neuroimaging

Antibodies

Antibodies used

Antibodies are annotated below as follows. WB, Western blot; IHC, immunohistochemistry. Dilutions are indicated. Any antibody validation by manufacturer is indicated and can be found on the manufacturers' websites.

Primary antibodies: ACSL4 (abcam, #ab155282, clone EPR8640, lot GR323574-1, WB, 1:1000, knockout-validated in-house), GPX4 (abcam, #ab125066, clone EPNCIR144, lot GR3369574-4, WB, 1:1000, validated by manufacturer), PRX (TXNRD1, PRX1, TRX) (abcam, #ab184868, , lot 2101027205, WB, 1:1000, validated in-house), CBS (Thermofisher, #MA5-17273, clone GT519, YF3959002B, WB, 1:1000, validated by manufacturer), CSE (Proteintech, #60234-1-Ig, clone 2C7F9, 10007221, WB, 1:1000, validated by manufacturer), POR (abcam, #ab180597, clone EPR14479(B), GR148691-13, WB, 1:1000, validated by manufacturer), FSP1 (Provided by Marcus Conrad, , clone #14D7, , WB, 1:1000,), FSP1 (Santa Cruz Biotechnology, sc-377120, clone B6, B0524, WB, 1:1000, validated in previous publication: 10.1038/s41586-023-06255-6), AGPS (abcam, ab236621, , 1095562-2, WB, 1:1000; IHC. 1:5000, knockout-validated in-house), FAR1 (Novus Biologicals, #NBP1-89847, , 34863, WB, 1:1000, knockout-validated in-house), ESR1 (Cell Signaling, 13826S, E1G1J, 4, WB, 1:1000, knockout-validated in-house), ETHE1 (GeneTex, GTX115707, , 40296, WB, 1:1000, validated in previous publication: 10.1038/s41589-022-01145-w), SQR (abcam, #ab71978, , 1013554-2, WB, 1:1000, validated in previous publication: 10.1038/s41589-022-01145-w), β-actin (Cell Signaling, #3700S, clone 8H10D19, 21, WB, 1:1000), GAPDH (Cell Signaling, #2118S, clone 14C10, 14, WB, 1:1000)

Secondary antibodies: Anti-mouse IgG; HRP-linked antibody (Cell Signaling, #7076S, , 38, WB, 1:5000), Anti-rabbit IgG; HRP-linked antibody (Cell Signaling, #7074S, , 33, WB, 1:5000; IHC, 1:200)

Validation

Information of antibody validation by manufacturers are indicated in the list above. Any antibody validation by the manufacturer is indicated and can be found on the manufacturers' websites. Our antibody validation strategy relies on using material from knockout cell lines or knockout mice (denoted as in-house in the list above). For some antibodies, we relied on the valdiation data provided in previous publications (publications specified in the list above).

Eukaryotic cell lines

Policy information about cell lines and Sex and Gender in Research

Cell line source(s)

HT1080 cells, NIH-3T3 cells, HT29 cells, and HeLa cells were obtained from the ATCC.
CD10-136 cells were generated in the Kramann laboratory (10.1016/j.biomaterials.2024.123009).

Authentication

Authentication was relied on by the commercial source where applicable (ATCC).
No authentication of human derived CD10 cells was performed. These cells were generated from primary sources directly in the Kramann lab. as published (10.1016/j.biomaterials.2024.123009).

Mycoplasma contamination

All cell lines were tested free of mycoplasma contamination regularly.

Commonly misidentified lines
(See ICLAC register)

None of the used cell lines are listed in the ICLAC register.

Animals and other research organisms

Policy information about studies involving animals; ARRIVE guidelines recommended for reporting animal research, and Sex and Gender in Research

Laboratory animals

All mice were kept under standard conditions in a controlled environment (12 h light/dark cycle, 22 ± 2 °C, 55 ± 5% humidity) with water and food ad libitum.
Wild-type controls were littermates to the respective mouse lines:
FSP1-ko (Aifm2tm1Marc), ESR1-mut (B6N(Cg)-Esr1tm4.2Ksk/J), MLKL-GSDMD-dko (MLKLtm1.2Wsa;C57BL/6N-Gsdmdem4Fcw/J), GPX4-ko (Gpx4fl/fl;ROSA26-CreERT2), CTH-ko (Cthtm1lish)
All other wild-type mice (C57Bl/6N) were initially provided by Charles River, Sulzfeld, Germany, at the age of 6 – 7 weeks.

	For animal studies, mice were randomised into separate cages. 8 to 12-week-old sex-matched mice were used for all experiments.
Wild animals	No wild animals were used in this study
Reporting on sex	Mammals, both male and female, used for this study are indicated in each figure legend.
Field-collected samples	No field samples were collected in this study.
Ethics oversight	If not otherwise specified, experiments were performed according to German Animal Welfare Law and were approved by the Institutional Committees on Animal Experimentation and local authorities in Dresden or Munich (Germany). All IRI and OVX experiments as well as organ harvesting have been approved by the government of Saxony (Landesdirektion Sachsen, LDS). Gpx4fl/fl;ROSA26-CreERT2 experiments have been approved by the government of Upper Bavaria (Regierung von Oberbayern). Experiments with Cthtm1lish mice have been approved by the local authorities in Lausanne. All experiments involving pigs were performed according to the German Animal Welfare Act with permission from the Government of Upper Bavaria, following the ARRIVE guidelines and Directive 2010/63/EU.

Note that full information on the approval of the study protocol must also be provided in the manuscript.

Plants

Seed stocks	*Report on the source of all seed stocks or other plant material used. If applicable, state the seed stock centre and catalogue number. If plant specimens were collected from the field, describe the collection location, date and sampling procedures.*
Novel plant genotypes	*Describe the methods by which all novel plant genotypes were produced. This includes those generated by transgenic approaches, gene editing, chemical/radiation-based mutagenesis and hybridization. For transgenic lines, describe the transformation method, the number of independent lines analyzed and the generation upon which experiments were performed. For gene-edited lines, describe the editor used, the endogenous sequence targeted for editing, the targeting guide RNA sequence (if applicable) and how the editor was applied.*
Authentication	*Describe any authentication procedures for each seed stock used or novel genotype generated. Describe any experiments used to assess the effect of a mutation and, where applicable, how potential secondary effects (e.g. second site T-DNA insertions, mosiacism, off-target gene editing) were examined.*

Flow Cytometry

Plots

Confirm that:

☒ The axis labels state the marker and fluorochrome used (e.g. CD4-FITC).

☒ The axis scales are clearly visible. Include numbers along axes only for bottom left plot of group (a 'group' is an analysis of identical markers).

☒ All plots are contour plots with outliers or pseudocolor plots.

☒ A numerical value for number of cells or percentage (with statistics) is provided.

Methodology

Sample preparation	Cells were harvested and the pellets were washed twice in PBS and stained with 5 µl of 7-AAD (BD Biosciences) and 5 µl of annexin-V-FITC (BD Biosciences) added to 100 µl annexin-V binding buffer solution (BD Biosciences). After 15 minutes, cells were recorded either on the Fortessa LSRII with the FACS Diva 6.1.1 software (BD Biosciences), or on the Symphony A3 with the FACS Diva v9.0 software (BD Biosciences) and subsequently analyzed with the FlowJo v10 software (Tree Star). The flow cytometry procedure was supported by the Flow Cytometry Core Facility of the CMCB Technology Platform at Technical University of Dresden (TU Dresden) and the FACS Facility of the Institute for Physiological Chemistry (TU Dresden). All data were analyzed with FlowJo software v 10.09.0
Instrument	BD Fortessa LSRII using FACS Diva 6.1.1 software BD Symphony A3 using FACS Diva v9.0 software
Software	FlowJo software v 10.09.0
Cell population abundance	At least 10000 events of single cells were measured for each sample.
Gating strategy	FSC/SSC were used to set the initial gate excluding debris but including dead cells. Doublets were excluded in sub-gates. The single-cell gate was recorded until 10,000 events were reached. Live cells correspond to 7-AAD and annexin V double

negative cells. A depiction of the gating strategy is provided in the Supplementary Information.

☒ Tick this box to confirm that a figure exemplifying the gating strategy is provided in the Supplementary Information.